Investigation of UV-VIS Converters Based on Erbium-Doped Aromatic Polyurethanes

by

Reyhane KILCI

A Thesis Submitted to the
Graduate School of Science and Engineering
in Partial Fulfillment of the Requirements for
the Degree of

Master of Science
in
Physics

Koç University

September 2008

Koç University

Graduate School of Sciences and Engineering

This is to certify that I have examined this copy of a master's thesis by

Reyhane KILCI

and have found that it is complete and satisfactory in all respects,
and that any and all revisions required by the final
examining committee have been made.

Committee Members:

_____

Alphan SENNAROĞLU, Ph. D. (Advisor)

_____

İskender YILGÖR, Ph. D.

_____

Alper KİRAZ, Ph. D.

Date: _____

ÖZET

Morötesi ışığı görünür ışığa çeviren erbiyum katkılanmış elastomerik poly (ether-urethaneurea) kopolimerlerinin spektroskopik ve renk özellikleri araştırıldı. % 5 ile % 25 aralığında $ErCl_3.6H_2O$ içeren polimer örnekleri sentezlendi. Katkılanmış erbiyum iyonlarından kaynaklanan soğurma bantları soğurma spektrumlarında gözlendi. Erbiyum katkılanmış polimerleri 355 nm dalga boyunda uyarınca görünür bölgede, 400–750 nm dalga boyları arasında geniş ışınım bantları elde edildi. Erbiyum iyonunun morötesini görünüre çevirmedeki etkisini araştırmak için farklı miktarlarda erbiyum iyonu içeren polimer örnekleri incelendi. Ayrıca, farklı erbiyum konsantrasyonlarındaki polimerler için renk koordinatları, renk verme indisi (CRI), gözün tepkisiyle örtüşme faktörü ve renk sıcaklığı değerleri belirlendi. Son olarak, erbiyum katkılanmış polimerlerin morötesini görünüre dönüştürme verimleri Rayleigh saçılması ve Fresnel kayıpları da göz önüne alınarak ölçüldü.

ABSTRACT

UV-to-visible conversion characteristics of novel erbium-doped elastomeric poly(ether-urethaneurea) copolymers were investigated. Polymer samples containing $ErCl_3.6H_2O$ at a concentration range of 5 to 25% by weight were synthesized. The absorption spectra of the samples showed bands due to the dopant erbium ions. When excited at 355 nm, the doped polymer samples produced emission covering the 400-750 nm visible region. Samples with different erbium concentrations were examined to compare the role of concentration in UV-VIS conversion. In particular, chromaticity coordinates, color rendering index (CRI), overlap factors with eye response, and color temperature were determined as a function of erbium ion concentration. Finally, conversion efficiencies of the erbium-doped polymers were investigated by accounting for Rayleigh scattering and Fresnel losses.

ACKNOWLEDGEMENTS

My first thanks are to my advisor Alphan Sennaroğlu, for his guidance and support. I would like to thank to İskender Yılgör and Alper Kiraz for their participation in my thesis committee.

I consider myself fortunate to have had marvelous friends; Zeynep Güler, Fatma Arık, Nilüfer Yılmaz, and Şeyma Zararsızsoy. I also thank to my friends who breathed the same air with me for these two years in Koç University; Gülay Ergül, Saliha Pehlivan, Zekiye Şahin, and Zeynep Akçay. Furthermore, I am thankful to Çiğdem and Mustafa Yorulmaz for their genuine friendship. Without the encouragement and motivation they have given to me during the past two years, it would not be possible to complete this thesis.

I am thankful to all my friends from Laser Research Laboratory; Natali Çizmeciyan, Serhat Tozburun, Ahmet Koray Erdamar. I also thank to Hamit Kalaycıoğlu, and Hüseyin Çankaya whose presence and ideas were a great source of me.

Finally and most importantly, I am grateful to my parents; Şükran, and Eyüp and my angels; Mercane and Leyla for their endless support and confidence throughout my education.

TABLE OF CONTENTS

LIST OF TABLES

LIST OF FIGURES

NOMENCLATURE

J	total angular momentum
L	total orbital angular momentum
S	total spin angular momentum
n	principal quantum number
l	orbital quantum number
$P(\lambda)$	spectral power distribution of light
c_i	total power absorbed by each cone
$s_i(\lambda)$	sensitivity of the i^{th} type of cone
$\bar{x}(\lambda)$	a color matching function
$\bar{y}(\lambda)$	a color matching functions
$\bar{z}(\lambda)$	a color matching functions
$x(\lambda)$	a chromaticity coordinate
$y(\lambda)$	a chromaticity coordinate
$z(\lambda)$	a chromaticity coordinate
$S(\lambda)$	spectral concentration of the incident radiant power
$\beta(\lambda)$	spectral reflectance properties of the object
X	a tristimulus value
Y	a tristimulus value
Z	a tristimulus value
k	normalization factor
x	a color coordinate
y	a color coordinate
z	a color coordinate
L*	a tristimulus value with variable changed
a*	a tristimulus value with variable changed

b^*	a tristimulus value with variable changed
ΔE_i	color difference for a sample
η	eye overlap index
T_C	color temperature of the object in Kelvin
A	absorbance
$R_e(\lambda)$	spectral response of the eye
L_F	Fresnel reflection loss
L_S	scattering loss
P_{flour}	fluorescence power
P_{in}	power inside the sample
T_L	transmission of the CaF_2 lens
R	spectral area ratio
β	solid angle ratio
P_{input}	power of the incoming light
η_{eff}	UV-VIS conversion efficiency

Chapter 1

INTRODUCTION

1.1: Overview of White Light Emitting Sources

White light emission has attracted a great deal of interest in science, technology, and daily life. There are widespread application areas of white light, for example, in architectural lighting, decorative lighting, flashlights, backlighting of large displays [1-7], full-color flat panel displays [8-10] and full-color micro-displays [6]. Automotive lighting [2], solid-state lighting, high efficiency active matrix displays are other crucial application areas. In active matrix displays, for example, full-color display is required in which red, green and blue colors are mixed with suitable chromaticity weights [2, 11].

Various approaches have been proposed for the generation of white light by using different materials and device architectures [1-8, 10-28]. One of them uses organic light emitting diodes (OLEDs) as emitting layers for which the thickness is controlled and adjusted for obtaining white light [2, 12, 13, 16]. Among these, an interlayer is found in between two luminescent layers and tuning of the spectrum -to achieve white light- can be obtained by changing the thickness of the interlayer [2]. As an example, Ko *et al*. [12] designed a bright white organic light-emitting diode consisting of different light emitting layers with various thicknesses. In Figure 1, the light-emitting diode can be seen with its layers. Each emitting layer radiates different colors such as Alq (tris(8-hydroxyquinolinato) aluminum (III)) layer emits green, PAP-Ph (1,7-diphenyl-4-biphenyl-3,5-dimethyl-1,7-dihydrodipyrazolo[3,4-b;4',3'-e] pyridine) emits blue, and also DCM (4-(dicyanomethylene)-2-methyl-6-(4-dimethylaminostyry)-4H-pyran)-doped Alq layer emits red. The thickness of the Alq layer is varied between 0 and 5 nm, and PAP-Ph is 5 nm. White emission can be obtained by adjusting the thicknesses of DCM doped Alq layer [12].

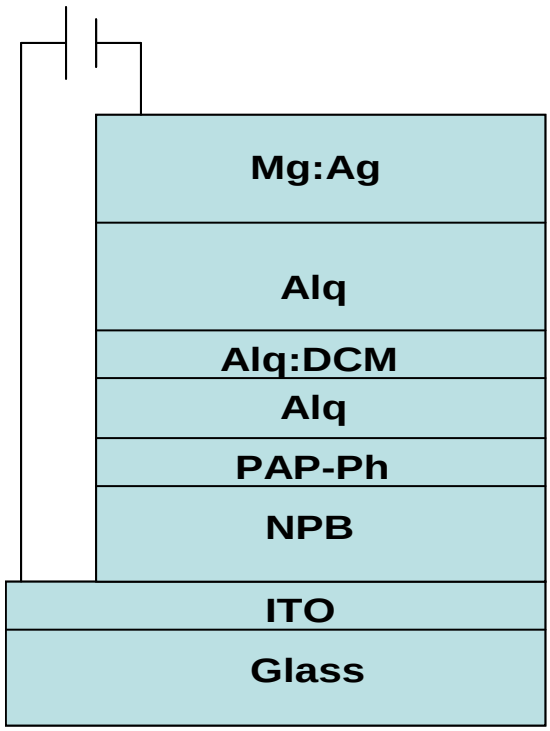

Figure 1.1: The configuration of the light-emitting diode multi-heterostructure adapted from Ko *et al.* [12]

To enable less expensive production, polymer light emitting diodes (PLEDs) generating white light are manufactured with spin-casting luminescent materials. Spin casting is a method for pouring the castings into a mold [16]. The other method for PLEDs is calibrating the concentration amount of polymer solid solutions to take narrow emission spectra of red, green, and blue colors for final white light [25]. Additionally, PLEDs based on blue and red phosphorescent polymers which are utilized as emissive layers are used with adjusted concentrations of phosphorescent polymers to reach white light emission [8]. In the topical review of Misra *et al.* [10] that is similar to the previous case, UV light is utilized to excite a number of phosphors which give different colors [10]. Mixing of colors gives white light that has the broadest spectrum and this process is called down-conversion by phosphors [10]. After the usage of conventional phosphors to obtain luminescence in the visible region [26], hybridized form of conjugated polymers and UV micro-LED arrays are utilized so that they convert the emission from ultraviolet InGaN LEDs to generate white light emission for

low-cost full-color microdisplays [6]. In order to obtain white light emission there are many advantages for conjugated polymers. For instance, they have strong UV absorption bands and the deposition of these materials is easy compared with phosphors [6].

In addition to these, thin films of ZnSe-grown by atomic layer deposition (ALD) which is an operation to form thin coatings- are excited by an electron beam to generate white light [17]. Whiteness of the fluorescence can be tuned by changing the accelerating voltage [18] or the excitation density [17].

As an alternative approach, single, dual, triple, and quadruple combinations of CdSe/ZnS nanocrystals (NCs) are hybridized with InGaN/GaN light emitting diodes (LEDs) to produce white light [4]. In this hybrid approach, the LED is used as the pump source and the NC film as the photoluminescent (PL) layer. After pumping of nanocrystals, the photoluminescence of nanocrystals and the electroluminescence of light emitting diodes (LED) combine to generate white light emission. Furthermore, with proper NC combinations involving single to quadruple components and with suitable sizes of NCs, visible spectrum can be completely covered [4]. Also, Chen *et al* [21] has done research about QDs and white light emitting diodes (WLEDs) that are close to previous work. In this research, WLEDs with three different bands –namely red, green, and blue - are combined with InGaN chips and CdSe-ZnSe QDs to obtain white light from WLEDs [21]. Besides, GaN quantum dots (QDs) grown on Si (111) substrate, give white light emission whose characteristics can be controlled by varying the size of QDs [24]. The other version of QD use in white light investigation is to obtain full-color emission by using QD-polymer composites which are excited by UV and the resulting spectrum covers the whole visible region [27]. This is obtained by combining the narrow emission band of each color and by controlling the mixing ratio of various sized QDs to obtain white light [27]. The color mixing method, which uses several emitters in one equipment to produce white light, is widely used [10]. In this technique, phosphors are not exploited in order to eliminate the losses that arise from the wavelength conversion [10].

To obtain high luminance and high luminous efficiency, organic EL devices are used [5]. Luminance and luminous efficiency are photometric quantities. Luminance defines the amount of light which is passed from a specific surface area and it has the SI unit of cd/m^2

[29]. Luminous efficiency, which depends on wavelength of light, is the fraction of luminous flux to the entire radiant flux. For instance, luminous efficiency of the human eye has a peak around 555 nm for daylight vision, called photopic vision, and also a peak around 510 nm for night-time vision, called scotopic vision [29]. Organic electroluminescent (EL) devices depend on multi-heterostructures with three light emitting dyes [3]. That is because most organic devices can only produce a single color of the spectrum [3]. By combining three different light emitting dyes, one can produce white light. In Figure 2, there is a structural shape of a blue organic EL device which is adapted from Hosokawa *et al* [14]. In this configuration, there is an emitting material DPVBi (4,4'-bis(2,2-diphenylvinyl) biphenyl). Luminance and luminous efficiency are high for this EL device. Blue EL devices are adjoined with color changing media (CCM) which are produced with the help of organic fluorescent media. Resulting multi-color emission for display technology can be obtained via CCM that alters the color of emission from blue to green or red [14].

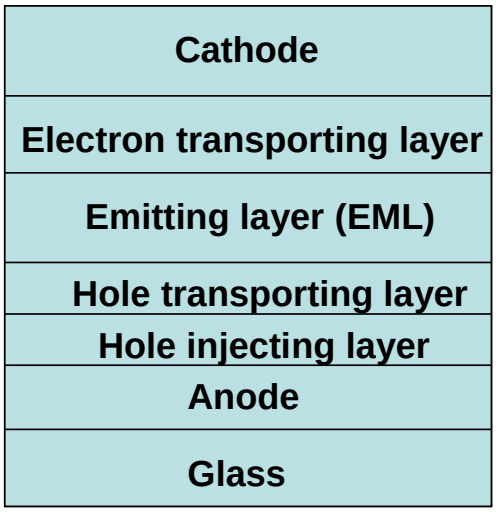

Figure 1.2: The architecture of the blue electroluminescent device which is adapted from Hosokawa et al [14].

As it can be seen, in that type of conventional white light emitters, red, green, and blue emitting materials are doped or fixed onto organic EL devices to obtain white light emission [5, 7]. However, controlling the peak intensities of each RGB emitter is very difficult and the device model is complicated. Because of this reason, for organic EL devices, white light

emitting material which emits white light by itself is preferred rather than RGB emitters [5]. Hamada et al. uses $Zn(BTZ)_2$ as white light emitting material which provides high reliability and productivity [5].

1.2 Description of the Methods Used in This Study

After providing a concise review of research done in white light generation, we now give a brief description of the method used in our studies. In this research, we have been investigating the light emission properties from erbium-doped polymers. Rare-earth doped polymers are used widely in fiber-optic communication systems, fiber laser development, optical sensing [28], integrated waveguides, and optical fiber amplifiers [30-32]. Additionally, proper selection of absorption and emission bands could be obtained because of wide selectivity range for rare-earth ions [28, 32]. For this study, we have explored the characteristics of white light emission from Er^{3+} doped aromatic polyurethanes under ultraviolet (UV) radiation (355 nm), for various concentrations of trivalent erbium ions. We have used erbium doped polymer samples as UV to visible converters. The reason of the selection of trivalent erbium ion is because of its several strong transitions in the visible portion of the spectrum [33]. In this experiment, we have generated 355-nm UV pump light by frequency tripling the output of a 1064-nm Nd:YAG laser. The visible emission of trivalent erbium ion near 550 nm is broadened to cover the 400-700 nm range as a result of phonon coupling with the polymer host. By studying the photoluminescence (PL) of these polymers with different Er^{+3} concentrations, we intend to determine the degree of whiteness of our samples.

Understanding the whiteness of our light sources has constituted a crucial part of the research. There are various analyses [2-6, 8, 10, 12, 13, 16, 17, 23-25, 27, 34] used for the characterization of white sources. These analyses consist of colorimetric inquiries which detect the closeness to the white region of color chart. White light emission covers the visible range of the spectrum which is in the interval of 380-780 nm. These white light emitters are utilized as UV-to-visible converters which have widespread application areas in science, technology, and industry.

Colorimetric analysis is based on the use of color coordinates which provide a quantitative measure for the visual perception system of a human. In the human eye, there is a part called retina which contains two types of photoreceptors: rods and cones. Rod photoreceptors which do not involve the color perception are for night vision of humans, and cone photoreceptors that perform the color perception are for day-time vision [35]. In the retina, there are three layers of cone photoreceptors by which the neural signal is sent to the brain to perceive incoming light and distinguish color differences clearly [35, 36]. These three cones correspond to red (R), green (G), and blue (B) which form the tristimulus measuring system**.** However, the denomination of red, green, and blue sensors may be misleading [35]. As such, red cones are sensitive mostly in the red-green portion of the spectrum [35]. Because of this, researchers denote the vision range of each photoreceptor (R, G, B photoreceptors) as long-wavelength sensitive (L), middle-wavelength sensitive (M), and short-wavelength sensitive (S) photoreceptors, respectively [35, 37]. L type cones peak around 570 nm, M cones around 545 nm, and S cones near 440 nm [35]. Cone sensitivity decreases outside the interval of 380-780 nm which is the visible portion of the spectrum of light. These three types of cones give the trichromatic generalization that symbolizes the additive mixture property of three primary lights [36, 37]. An observer could match every spectral light that is in different wavelengths with the addition of all spectral components of light to attain the final display of the image [37]. The final display is obtained with the coalescence of each partial catch that is produced by the three primary lights in each of the three cone photoreceptors [37]. It means that one could afford to match any spectral light by using each of the three types of cones which have different sensitivity [37]. To realize the relationship between matching intensities of the three primary lights and the wavelength of the spectral light [36], the color matching functions (CMFs) were established in 1931 by CIE (Commission Internationale de L'eclairage; International Commission on Illumination) [36]. The CIE organization has been putting predetermined regulations on colorimetric and photometric standards since 1931.

Color matching functions (CMFs) are utilized in all calculations for taking tristimulus values and color rendering index (CRI) of each sample. The tristimulus values of a light

source are the results of the relationship between three cones with three primary lights to describe true visual perception of a human. The tristimulus values evaluate the amount of red, green, and blue primaries present to match a color to the light of an illuminant. At first, the color coordinates, which are the basic way of describing the color of light, are found from multiplication of the predetermined CMFs and the spectral power distribution of the light source. From the tristimulus values, we can reach the final color coordinates of any illuminant. Also, color chart is obtained by implementing the chromaticity coordinates, to observe the closeness of color coordinates to the white point of the horseshoe shape of chromaticity diagram. At that point, from comparison of the tristimulus values of our illuminant and any type of standard daylight illuminant gives the resulting color rendering index (CRI) which represents the rendition of colors for an object by an illuminant. That is the vividness quality of the illuminated samples and the representation factor of each color, effectively. It can take its value between 0 and 100, where '100' means maximal rendition of colors and '0' means complete distortion of colors. Furthermore, the color temperature (CT) of a light source, which is found from the Wien's Displacement Law, indicates the color quality of the source in comparison with an ideal blackbody radiator. This law testifies that maximal intensity wavelength of blackbody radiation is inversely proportional to the absolute temperature. One can find the temperature of each color of light from the determination of maximal intensity in the emission spectrum [38]. Additionally, there is an overlap factor (η) which denotes the degree of resemblance between the emission spectrum of the samples and eye response curve.

1.3 The Structure and Characterization of Polymers

All organic compounds absorb UV light [39]. However, aliphatic polymers absorb below 220 nm [40, 41] and aromatic compounds have more definite absorption bands in the region of 200-400 nm [40, 42, 43]. Because of this reason, the UV excitation spectroscopy is typically applied to aromatic compounds [40, 42, 43]. The main reason is the presence of benzene rings in aromatic compounds, which strongly absorb UV, whereas the aliphatic ones do not. UV radiation in 200-400 nm wavelengths can penetrate through aliphatic polymers without

being absorbed [41]. In addition to benzene rings [42] some other groups or chromophores also absorb UV [39, 41]. In this study, we utilized an aromatic polyurethaneurea as the host material which contained benzene rings, which were bonded to each other with a methylene group. Chemical structure of the segmented polyurethaneurea copolymer is provided below in Figure 1.3.

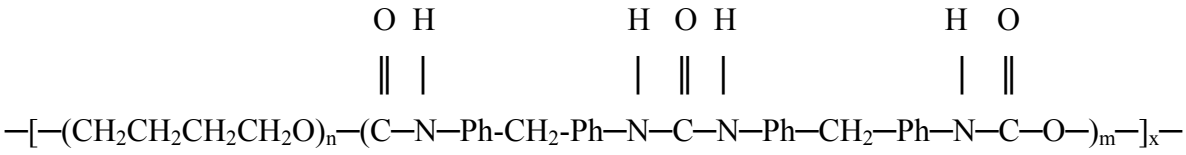

Figure 1.3: The representation of the polymer chain.

In this formula 'n' and 'm' represent the average number of various repeating units along the macromolecular backbone and 'x' represents the average degree of polymerization.

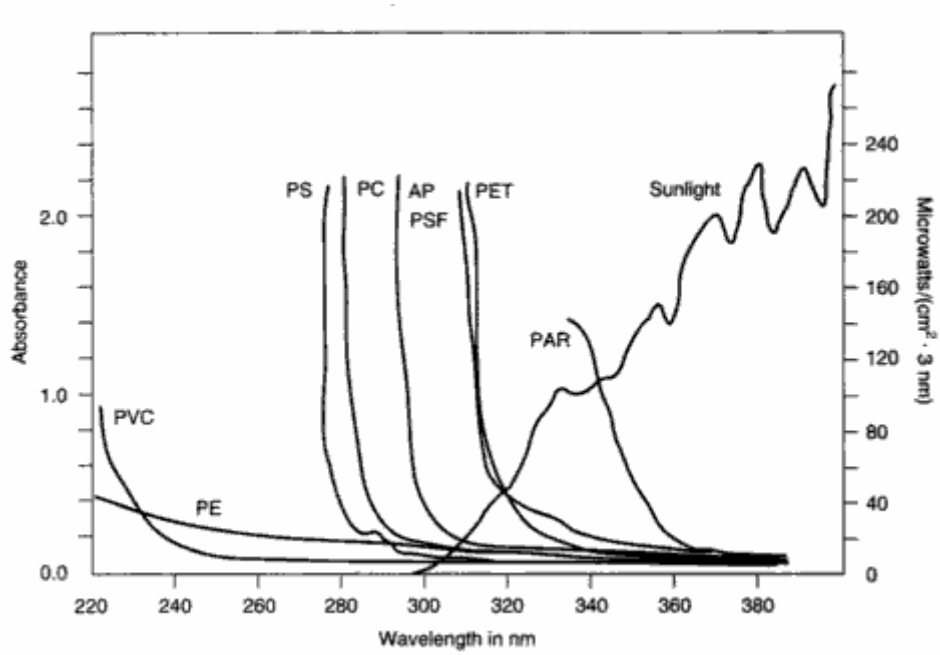

Figure 1.4: Absorption spectra of various polymer films and spectral irradiance for July noon sunlight at 41° latitude. AP: Aromatic polyester [41].

As shown in Figure 1.4. aromatic polymers involve chromophores which sometimes are responsible for giving color to a compound and these chromophores have absorption bands at wavelengths usually longer than 290 nm [41]. Andrady *et al*. [41] point out that absorption band of aromatic polyester is close to 300 nm (Figure 1.4).

The chromophore present in the polyurethaneurea is the carbonyl (C=O) group. Carbonyl group has an absorption band near the wavelength of 280 nm [39], which is close to our excitation wavelength of samples. Benzene which has an absorption band around 255 nm (Figure 1.5) is one of the UV absorbing compounds [42].

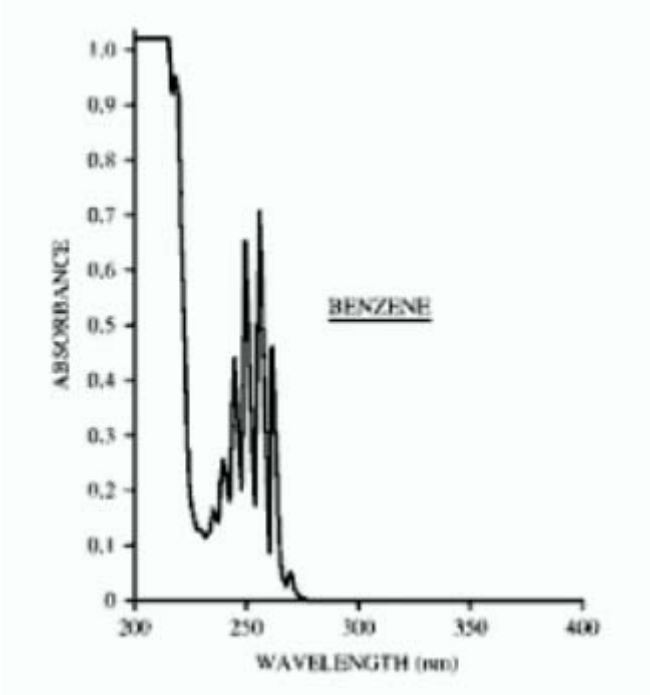

Figure 1.5: UV absorption spectrum of Benzene [42]

In this investigation, we should note that absorption bands are seen in the spectrum as opposed to absorption lines, since vibrational and rotational effects are seen on the electronic transitions and there is an envelope of transitions [39]. As an example, benzene ring, which is the main constituent in aromatic polymers, is influenced by vibrational and rotational effects. In vapor phase, fine structure can be seen obviously, but in liquid or solid phase, the transitions are not seen exactly [39] and the spectrum is broadened.

1.4. Erbium Spectroscopy

Trivalent rare-earth elements have the electronic configuration $[\mathrm{Xe}]\,4f^{N-1}5s^2 5p^6 6s^0$ in which [Xe] symbolizes the electronic configuration of the element Xenon [44]. For trivalent rare-earths, one and two electrons are separated from $4f$ and $6s$ shells. Also, there are $N-1$ electrons in the $4f$ shell which is protected from the effects of $5s$ and $5p$ electrons. As a result of this property, there can be $4f \rightarrow 4f$ transitions to provide sharp absorption and emission lines. The other benefit of this is that the spectroscopic features of the $4f \rightarrow 4f$ transitions are not greatly influenced by the particular host [44].

The energy level structure of elements can be explained by quantum theory [44]. We have $N = 12$ for the element Erbium, which means that in the $4f$ shell of the Er^{+3} ion, there are 11 electrons [44, 45]. Quantum atomic states of an electron are specified by four quantum numbers which are represented as "n, l, m, s". "n" is the principal quantum number ($n = 0,1,2...$) and it expresses the radial probability distribution density of an electron. "l" is the orbital quantum number which takes values between 0 and n-1. It gives the total angular momentum of an electron as $\sqrt{l(l+1)}\hbar$. We can identify the orbital quantum numbers as $s, p, d, f, g, h, i...$ for $l = 0,1,2,3,4,5,6...$, respectively [44]. Furthermore, "m" shows the orbital angular momentum orientation and takes integer values between $-l$ and $+l$ altogether $2l+1$ possible values. These identifications are done for one electron. For multi-electron atom, we use the symbol "J" to designate the total angular momentum. J is given by

$$J = L + S \tag{1.1}$$

In the above formula, L is the sum of the total orbital angular momentum that should take an integer value, and S is total spin angular momentum that can be integer or half-integer. Collection of the quantum states of a multi-electron system are described by the numbers (J, L, S), and multiplicities are $2J+1$ for total angular momentum and $2S+1$ for total spin of a multi-electron atom. While representing the energy levels of the atom, we define the states with the symbol ${}^{2S+1}L_J$ in which $L = 0,1,2,3,4,5,6...$ refers to

$S, P, D, F, G, H, I...$, respectively [44]. For instance, $^4I_{15/2}$ has the quantum number set $(\ 15/2, 6, 3/2\ )$ and it has multiplicities $2J+1=16$ and $2S+1=4$ for which we can say that there are 16 allowed energy levels for L=6 angular momentum level [44].

There are degenerate states in the same atomic energy levels. For the above example in level L=6, there are 16 degenerate states. The degeneracy is lifted by the Coloumb interaction, spin-orbit coupling, and the Stark effect [46, 47]. First two effects are related with the free atom, but the third effect originates from the external electric field due to the crystalline or polymer host. If there is an external magnetic effect, degeneracy is lifted by the Zeeman effect [44, 45].

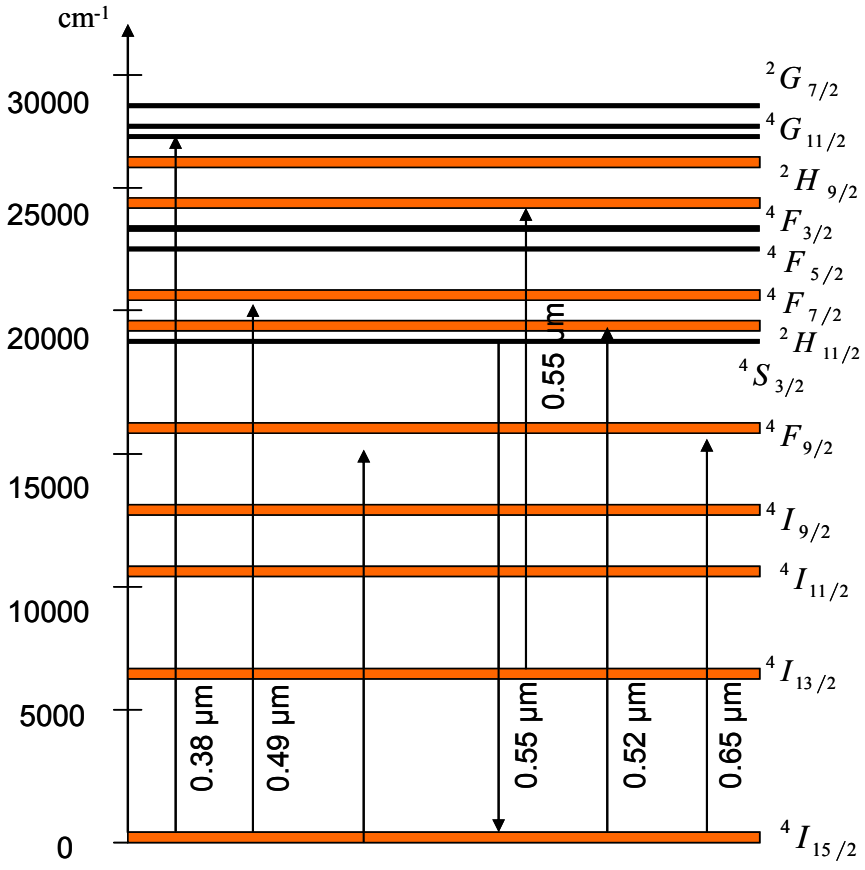

Figure 1.6: Energy levels of the Er^{3+} ion

Er^{3+} ion has various absorption lines which are shown in Figure 1.6. Examples include $^4G_{11/2} \rightarrow {}^4I_{15/2}$, $^4F_{5/2} + {}^2H_{9/2} \rightarrow {}^4I_{15/2}$, $^4F_{7/2} \rightarrow {}^4I_{15/2}$, $^2H_{11/2} \rightarrow {}^4I_{15/2}$, $^4S_{3/2} \rightarrow {}^4I_{15/2}$, $^4F_{9/2} \rightarrow {}^4I_{15/2}$, $^4I_{9/2} \rightarrow {}^4I_{15/2}$, $^4I_{11/2} \rightarrow {}^4I_{15/2}$ transitions which correspond to absorption at the wavelengths of 380, 430, 490, 520, 550, 650, 800, and 900 nm, respectively [48]. In the trivalent erbium doped polymer samples used in this study, the observed band is possibly due to the 520, 550, and 650 nm emission bands of Er^{3+} that correspond to the $^2H_{11/2} \rightarrow {}^4I_{15/2}$, $^4S_{3/2} \rightarrow {}^4I_{15/2}$, and $^4F_{9/2} \rightarrow {}^4I_{15/2}$ transitions, respectively. The vibrational and rotational interactions broaden the spectrum around 550 nm through the spectral region from 400 to 750 nm. Furthermore, the samples are excited at 355 nm by using the third harmonic of the Nd:YAG laser. The experimental setup and procedure will be explained in Chapter 3.

In this thesis, we have investigated the emission properties of erbium doped polyurethanes and the color characteristics of each sample for potential applications as a UV-to-visible converter. The analyses used in the characterization of the degree of whiteness will be explained in Chapter 2. Details of the experimental setup will be discussed in Chapter 3.

Chapter 2

THEORY OF COLOR ANALYSIS

In colorimetry, there are various methods used in order to quantify the degree of whiteness of light sources. The origin of these methods is based on the concept of color and the color visualization by humans. In this Chapter, the elements of visual system and their contributions to color perception are first introduced. Then, various measurement methods are defined and explained. These include the determination of the (x, y) color coordinates, eye overlap index, color temperature, and color rendering index. The calculation methods of these parameters are described in detail. First, we start with the definition and visualization of color.

2.1. Color Vision

Color is an interpretation of light by human beings. Due to this, color is not a physical property [35]. If color depends on how a human perceives light, we should establish a definition of color based on human color perception. One important characteristic of color is its invariability under a varying light intensity [35]. For example, when we place a painting under a light of modulated intensity, we can see that there is no change in the color of the painting [35]. One can thus conclude that color is a property which is invariant under changing light intensity [35].

The perception of color is formed with a physical stimulus initiated by electromagnetic radiation in the 380-780 nm wavelength range. After the stimulation of the eye, various elements of the eye and the brain also enter the picture for color perception. In color vision, the light is focused through the retina by the cornea and the lens of the eye. Retina is the outgrowth of the brain in the back part of the eye [35]. There are photoreceptors in the retina which sense the image. After the formation of neural signals which are transmitted to the brain, the sensation and visualization of any display can be obtained. There are two kinds of

photoreceptors known as rods and cones [35, 49, 50]. To form scotopic vision, rods are utilized, which are very sensitive to light even if the light intensity is very low [50]. In scotopic vision, there is no color perception, since it is called night-time vision [35]. In photopic vision which is called day-time vision [35], cones are active. That event can be explained with the saturation of rods because rods are highly sensitive to light. This situation gives way to the use of the less-sensitive cones for day-time vision [50].

In retina, there are three layers of cone photoreceptors to capture light and convert it into a neural signal which is sent to the human brain [35, 36]. The three types of cones are red (R), green (G), and blue (B). Within this designation, long-wavelength sensitive (L), middle-wavelength sensitive (M), and small-wavelength sensitive (S) meanings are also used for R, G, B, respectively [35, 37]. These cones have different peak wavelengths at 570 nm, 545 nm, and 440 nm for L, M, and S, respectively [35]. The sensitivity of each type of cone is represented in Figure 2.1 [50].

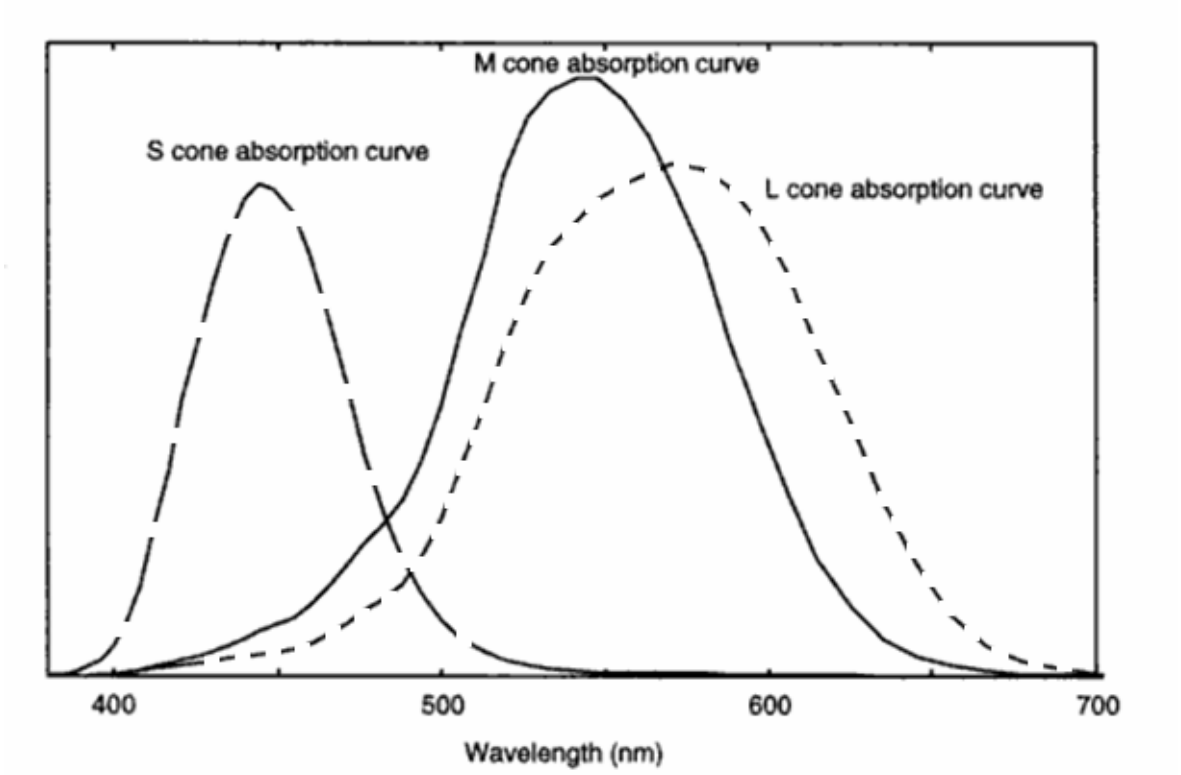

Figure 2.1: The spectral sensitivities of the three types of cones (S, M, and L). The figure is adapted from Reference [35].

We can express the total power absorbed by each cone with a linear system of equations which is given by $c_i = \int_{\lambda_{\min}}^{\lambda_{\max}} s_i(\lambda)P(\lambda)d\lambda$, where $P(\lambda)$ is the spectral power distribution of light, λ is the wavelength of the light, $s_i(\lambda)$ is the sensitivity of the ith type of cones, and $i = 1,2,3$ [35, 50]. Outside of the $\lambda_{\min}$ - $\lambda_{\max}$ range for human eye, sensitivities of cones are at the minimum level [35, 50].

In order to define color stimuli with all of its light components, one can describe it with vectors in a three dimensional space which is called the tristimulus space [36]. The vectors are denoted by **Q**, **R**, **G**, and **B [36]**. **Q** symbolizes an arbitrary color stimulus and **R**, **G**, **B** are used as the fixed primary stimuli. This concept is selected as a basis of color-matching. The spectral distribution of the arbitrary stimuli **Q** is represented as $\{P_\lambda d\lambda\}_Q$. Similar notations are utilized for primary stimuli which are R, G, and B:

$$\{\rho P_\lambda d\lambda\}_R \text{ is for R} \quad , \tag{2.1}$$

$$\{\gamma P_\lambda d\lambda\}_G \text{ is for G} \quad , \tag{2.2}$$

$$\{\beta P_\lambda d\lambda\}_B \text{ is for B} \quad . \tag{2.3}$$

ρ, γ, β are positive weighting factors for each color range. With the help of these values, we can figure out a color match by the equation:

$$\mathbf{Q}=R_Q\mathbf{R}+G_Q\mathbf{G}+B_Q\mathbf{B} \quad . \tag{2.4}$$

In Equation 2.4, R_Q, G_Q, B_Q are found from the units of primary stimuli. We can define the arbitrary stimuli for each monochromatic wavelength as $\mathbf{Q}_\lambda$ and the formula becomes

$$\mathbf{Q}_\lambda = R_\lambda\mathbf{R}+G_\lambda\mathbf{G}+B_\lambda\mathbf{B}. \tag{2.5}$$

These R_λ, G_λ, B_λ are called spectral tristimulus values. We can express it as

$$\mathbf{Q}(\lambda) = r(\lambda)\mathbf{R}+g(\lambda)\mathbf{G}+b(\lambda)\mathbf{B}. \tag{2.6}$$

The lowercase letters stand for spectral tristimulus values [35, 36]. The general power distribution is represented by

$$Q(\lambda) = Rr(\lambda) + Gg(\lambda) + Bb(\lambda). \tag{2.7}$$

We can write $P(\lambda)$ instead of $Q(\lambda)$. Total power absorbed by each cone can be calculated from

$$a_L = \int L(\lambda)P(\lambda)d\lambda \tag{2.8}$$

$$a_L = R\int L(\lambda)r(\lambda)d\lambda + G\int L(\lambda)g(\lambda)d\lambda + B\int L(\lambda)b(\lambda)d\lambda \tag{2.9}$$

$$a_M = \int M(\lambda)P(\lambda)d\lambda \tag{2.10}$$

$$a_M = R\int M(\lambda)r(\lambda)d\lambda + G\int M(\lambda)g(\lambda)d\lambda + B\int M(\lambda)b(\lambda)d\lambda \tag{2.11}$$

$$a_S = \int S(\lambda)P(\lambda)d\lambda \tag{2.12}$$

$$a_S = R\int S(\lambda)r(\lambda)d\lambda + G\int S(\lambda)g(\lambda)d\lambda + B\int S(\lambda)b(\lambda)d\lambda . \tag{2.13}$$

These equations of a_L, a_M, a_S define the powers of three different cone absorptions. These parameters represent the absorbed power by each cone at various proportions of the spectrum with various absorption amounts. It means that absorption for each cone is defined with the combination of three primaries. Trichromacy is the addition of these three primaries of light [35, 36]. Sensation of color is obtained through the comparison of three cone types which have different spectral sensitivities. These spectral comparisons are done in the neural branch of the retina. A standard normal observer, who has all three types of cones, could afford to match any spectral light in terms of three fixed color primary lights and one of them is contributed to the spectral light to form a complete match. The match is obtained in cones with the help of the produced partial catch in three primaries in three different cone types which is the same as the partial catch for the spectral test light. There are three functions that associate matching intensities with the wavelength of the three primary lights known as color matching functions.

To form a final vision from trichromats, these color-matching functions have been determined by the CIE (Commission Internationale de l'Eclairage) which announced its first standardization in 1931 [36]. 1931 standardization was used until 1971. CIE 1931 standard generated color-matching functions $\bar{x}(\lambda)$, $\bar{y}(\lambda)$, $\bar{z}(\lambda)$. In 1931, these functions were described at $\Delta\lambda = 5\,\text{nm}$ wavelength intervals between 380-780 nm. The new standard

introduced in 1971 was almost the same but there were some interpolated data in 5 nm ranges to take 1 nm interval list of data for color-matching functions which was in the range 360-830 nm. The graph of $\bar{x}(\lambda)$, $\bar{y}(\lambda)$, $\bar{z}(\lambda)$ color-matching functions are shown in Figure 2.2, 2.3, and 2.4.

In addition, there were $x(\lambda)$, $y(\lambda)$, $z(\lambda)$ chromaticity coordinates in the 1971 standard with upgraded significant figures for color-matching functions [36]. Chromaticity coordinates are the ratio of each color matching function to the sum of them for each wavelength in the range of 360-830 nm. Chromaticity coordinates are important for figuring out the color chart which will be explained in section 2.3.

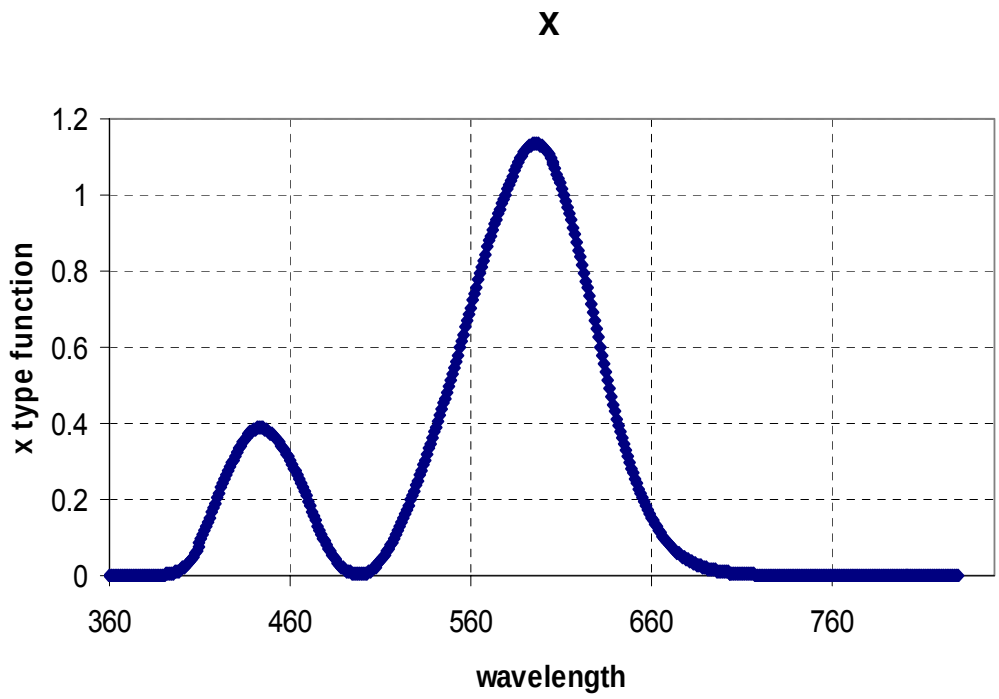

Figure 2.2: Spectral distribution of the $\bar{x}(\lambda)$ color matching function.

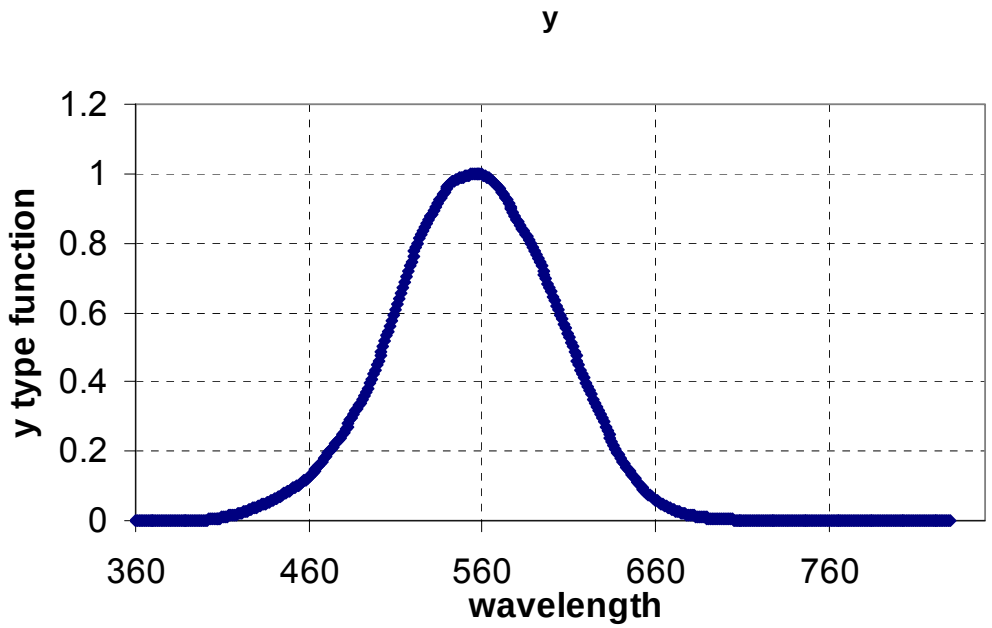

Figure 2.3: Spectral distribution of the $\bar{y}(\lambda)$ color matching function.

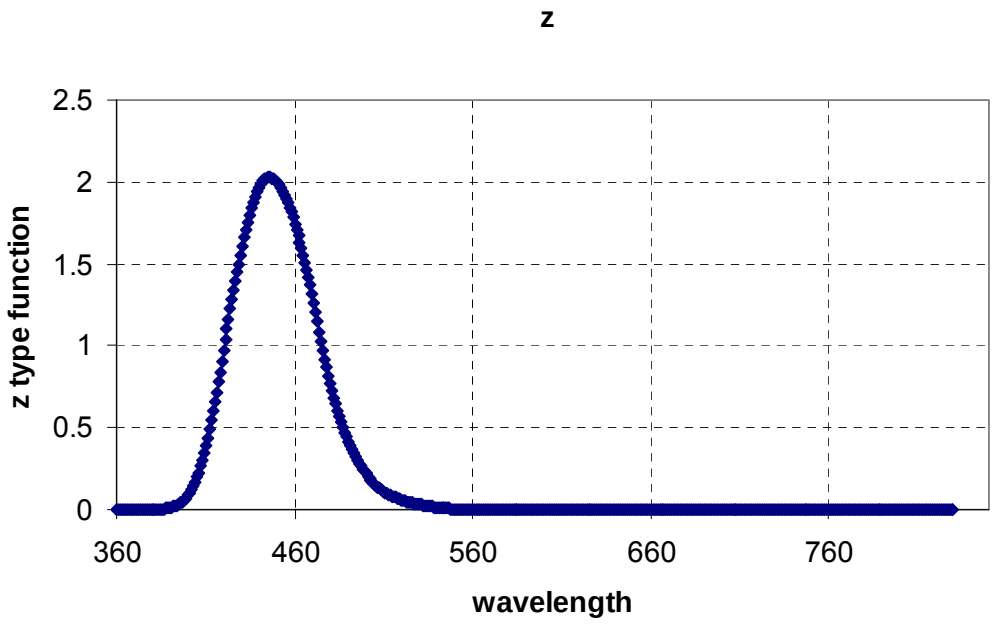

Figure 2.4: Spectral distribution of the $\bar{z}(\lambda)$ color matching function.

2.2. Calculation Method for the Color Coordinates (x, y, z)

Light emanated from the illuminant hits an object and makes the object visible to the observer. Object-color stimulus **Q** enters into the eye of the observer to provide the perception of the color of the object. $\{P_\lambda d\lambda\}$ is spectral radiant power distribution of the object-color stimulus **Q** which should be equal to $\{\beta(\lambda)S_\lambda d\lambda\}$. S_λ represents the spectral concentration of the incident radiant power and $\beta(\lambda)$ represents the spectral reflectance properties of the object. That reflectance property is originated from the three related concepts in color vision. These three concepts are light source, object, and human visual system. The reflectance property expresses the importance of the inclusion of the object in the reflection of light. $\{P_\lambda d\lambda\}$ is related to S_λ and $\beta(\lambda)$ through

$$\{P_\lambda d\lambda\} = \{\beta(\lambda)S_\lambda d\lambda\} \ . \tag{2.14}$$

In this set of calculations, color matching functions which are in the range of 360-830 nm have predetermined data in CIE records. In our calculations, we used the CIE 1964 data standards from Color & Vision Research Laboratories in UCL (University College London) [58]. Also, D65 daylight illuminant was used which is one of the CIE standard illuminants. The equations used for finding the tristimulus values X, Y, Z, are [36]

$$X = k\int_\lambda P_\lambda x'(\lambda)d\lambda \quad , \tag{2.15}$$

$$Y = k\int_\lambda P_\lambda y'(\lambda)d\lambda \quad , \tag{2.16}$$

$$Z = k\int_\lambda P_\lambda z'(\lambda)d\lambda \quad , \tag{2.17}$$

where “k” is a normalization factor of tristimulus values obtained by setting Y equal to 100:

$$k = \frac{100}{\int_\lambda S(\lambda)y'(\lambda)d\lambda} \ . \tag{2.18}$$

This normalization was done to provide a comparison of various samples' tristimulus values. The resulting color coordinates x and y were calculated from

$$x = \frac{X}{X+Y+Z} \quad , \tag{2.19}$$

and

$$y = \frac{Y}{X+Y+Z} \quad . \tag{2.20}$$

x, y, z values are the color coordinates of an illuminant and designate the region where the illuminant falls inside the color chart. The color chart was drawn by using the chromaticity coordinates. That analysis is a bit different for self-luminous color stimulus where the tristimulus values can be expressed as

$$X = k\Sigma S(\lambda)x'(\lambda) \quad , \tag{2.21}$$

$$Y = k\Sigma S(\lambda)y'(\lambda) \quad , \tag{2.22}$$

and

$$Z = k\Sigma S(\lambda)z'(\lambda) \quad . \tag{2.23}$$

For self-luminous color stimulus, we did not use $\beta(\lambda)$ reflectance coefficients, since we did not send light through the test samples. We measured only self-luminosity properties of our samples. The determination of "k" is the same for this investigation:

$$k = \frac{100}{\Sigma S(\lambda)y'(\lambda)} . \tag{2.24}$$

Moreover, the color coordinates were determined by using the following formulas:

$$x = \frac{X}{X+Y+Z} \quad , \tag{2.25}$$

$$y = \frac{Y}{X+Y+Z} \quad , \tag{2.26}$$

where

$$x + y + z = 1 \quad . \tag{2.27}$$

For self-luminous color analysis, we applied these formulae to determine tristimulus values of the erbium-doped polymer illuminants. After finding the (x, y) color coordinates, we determined the degree of whiteness by testing whether or not the coordinate falls within the white region of the color chart. The inclusion of the "k" parameter does not affect the final result of color coordinates, since it appears both in the numerator and denominator of the expressions for x and y.

2.3. Color Chart

By using equations (2.21), (2.22), and (2.23), we can reach color chart plot in which $S(\lambda)$ is taken as the δ-function and the value of "k" cancels out as discussed above. The resulting tristimulus values and color coordinates are given by

$$X_i = x_i'(\lambda) \quad , \tag{2.28}$$

$$Y_i = y_i'(\lambda) \quad , \tag{2.29}$$

$$Z_i = z_i'(\lambda) \quad , \tag{2.30}$$

and

$$x_i = \frac{X_i}{X_i + Y_i + Z_i} \quad , \tag{2.31}$$

$$y_i = \frac{Y_i}{X_i + Y_i + Z_i} \quad , \tag{2.32}$$

$$x_i + y_i + z_i = 1 \quad . \tag{2.33}$$

We used (x, y) values of these results to plot the two dimensional color chart. After plotting the color chart, we joined the two end points of the horseshoe-shape curve as shown in Fig. 2.5. The resulting (x, y) values are equal to the chromaticity coordinates [58].

The commonly accepted white region of the color chart is near the center within an ellipsoidal boundary. We used the article by Godlewski *et al.* [17] to obtain a least squares fit to the ellipse. The best-fit curves for the lower and upper sections of the ellipse are given by

$$y \to 5.20516 \times 10^{-7} \left\{ 197370 + 895200 \times x - 1.74881 \times 10^{6} \sqrt{-0.112898 + 0.718248x - x^2} \right\}$$

and (2.34)

$$y \to 5.20516 \times 10^{-7} \left\{ 197370 + 895200 \times x + 1.74881 \times 10^{6} \sqrt{-0.112898 + 0.718248x - x^{2}} \right\}$$

This ellipse can be seen in Figure 2.5 inside the color chart.

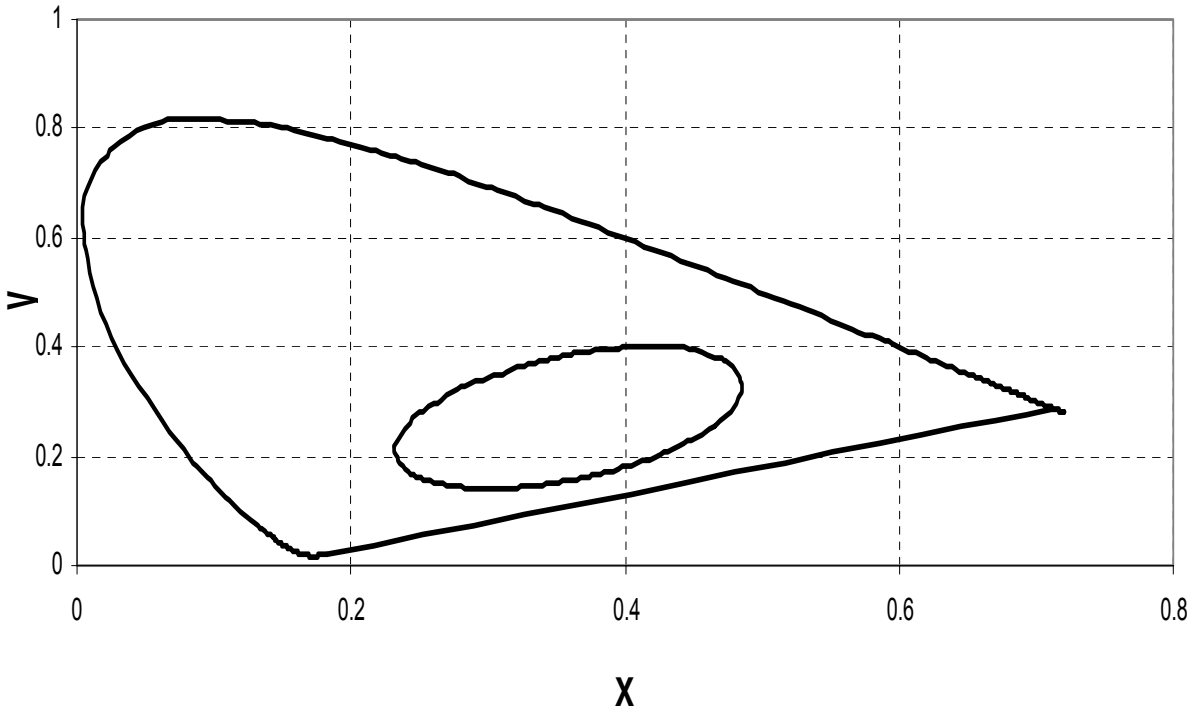

Figure 2.5: Color chart plot drawn by using the x, y color matching functions.

2.4. Color Rendering Index Calculation

Color rendering index (CRI) of a light source is a measure of the rendition of colors with the comparison between our illuminant and a reference illuminant. It means that CRI is the resemblance degree of the perceived colors from an illuminated object in comparison with another illuminated object which is illuminated by a standard light source [36, 49]. It articulates to what amount a light source renders the colors of an object. It can be illuminated under the selected light source and the comparison is done with daylight source. To obtain the results of color rendering index, one should determine object-color perceptions and differences with a standardized light source which are published by CIE. CRI takes the value

in between 0 and 100, where 100 means the maximal rendition of colors and 0 means the full distortion of colors.

There are eight test-color samples with specific spectral reflectance factors. These predetermined samples express colors under light illumination according to their own reflectance coefficients for each wavelength of light. Their different appearance under daylight is expressed in Table 2.1.:

Sample No	Color Appearance Under Daylight
1	Light grayish red
2	Dark grayish yellow
3	Strong yellow-green
4	Moderate yellowish green
5	Light bluish green
6	Light blue
7	Light violet
8	Light reddish purple

Table 2.1: Color Appearances of eight test-color samples adapted from Wyszecki *et al*. [36].

We should measure X, Y, Z tristimulus values of the test-color samples by using equations (2.15), (2.16), and (2.17). To take the CRI value, we should obtain a color difference formula which consists of the differentiation of luminescence of our light source and standard illuminant. To obtain the measurement of CRI, we make a change of variables from X, Y, Z to L*, a*, b* [36] according to

$$L^* = 116\left(\frac{Y}{Y_n}\right)^{1/3} - 16 \quad , \tag{2.35}$$

$$a^* = 500\left[\left(\frac{X}{X_n}\right)^{1/3} - \left(\frac{Y}{Y_n}\right)^{1/3}\right] \quad , \tag{2.36}$$

$$b^* = 200\left[\left(\frac{Y}{Y_n}\right)^{1/3} - \left(\frac{Z}{Z_n}\right)^{1/3}\right] \quad . \tag{2.37}$$

In these formulas, we have used X, Y, Z for tristimulus values of self-luminous color stimulus, and X_n, Y_n, Z_n for the tristimulus values of object-color stimulus of eight different test-color samples. We should use $\beta(\lambda)$'s of each of the eight test-color samples to determine the tristimulus values of our illuminant and D65 source for each sample [36]. Furthermore, $S(\lambda)$ values are the spectral concentration of the radiant power of our analyzed illuminant. X, Y, Z, x, and y are calculated as before:

$$X = k\int_{\lambda} \beta(\lambda)S(\lambda)x'(\lambda)d\lambda\,, \quad Y = k\int_{\lambda} \beta(\lambda)S(\lambda)y'(\lambda)d\lambda\,, \quad Z = k\int_{\lambda} \beta(\lambda)S(\lambda)z'(\lambda)d\lambda\,, \tag{2.38}$$

$$k = \frac{100}{\int_{\lambda} S(\lambda)y'(\lambda)d\lambda}\,, \tag{2.39}$$

$$x = \frac{X}{X+Y+Z}\,, \qquad y = \frac{Y}{X+Y+Z}\,, \tag{2.40}$$

We have used these tristimulus values of self-luminescence and object-color stimulus in the L*, a*, b* calculations and later in color difference formula:

$$\Delta E^*_{ab} = \left[(\Delta L^*)^2 + (\Delta a^*)^2 + (\Delta b^*)^2\right]^{1/2}, \tag{2.41}$$

$$\Delta E^*_{ab} = \left[(L^* - L^*_{ref})^2 + (a^* - a^*_{ref})^2 + (b^* - b^*_{ref})^2\right]^{1/2}. \tag{2.42}$$

In final formula, we took self-luminous tristimulus values as reference coordinates; L^*_{ref}, a^*_{ref}, b^*_{ref} for which there is no need to include $\beta(\lambda)$ coordinates, the object-color stimulus coordinates for eight samples as L*, a*, b* [36]. After finding eight ΔE_i for eight test-color samples, we used the following formulas to calculate the color rendering index R_a of each sample:

$$R_i = 100 - 4.6(\Delta E_i) \tag{2.43}$$

$$R_a = \frac{1}{8}\sum_{i=1}^{8} R_i\,. \tag{2.44}$$

2.5. Eye Overlap Index Calculation

We introduced an additional parameter which we denote as the η factor to investigate the degree of overlap between the spectral eye response function and the spectrum of the emitter. The η factor can be determined from the formula below:

$$\eta = CosQ = \frac{A \bullet B}{AB} = \frac{\sum_i A_i \bullet B_i}{\sqrt{\sum_i |A_i|^2}\sqrt{\sum_i |B_i|^2}} \tag{2.45}$$

In this formula, A, and B represent two spectral radiance functions measured at discrete wavelength points. The particular spectra used in our case were measured at 1-nm intervals. The proximity of η to the value of "1" expresses the degree of resemblance of our spectra with the response of the eye. We had different η values between 0.85-0.95. In this investigation, the data of the eye response were taken from Newport [57]. However, data were not taken in 1 nm interval. Because of this, we did a fit to this graph by using a function of the form:

$$y = y_0 + \left(\frac{A}{\left[w\sqrt{\pi/2} \right]} \right) \exp\left(-2\left[\frac{x - x_c}{w} \right]^2 \right) \tag{2.46}$$

In that formula, $y_0 = -0.00036$, $x_c = 559.07787$, $w = 83.86405$ and $A = 106.88382$.

Afterwards, we were taken the response data in 1 nm interval, and new response graph and data were utilized for eye overlap index calculation. The response graph will be seen in Figure 2.8 which is drawn with the addition of S2 sample (2.19% Er^{3+} doped one).

2.6. Color Temperature Calculation

Color temperature is found from Wien's Displacement Law which is stated by Wilhelm Wien in 1893 for a blackbody. It establishes a relationship between wavelength maxima of the blackbody radiation and its temperature. The hotter the blackbody, the shorter the wavelength maxima of the radiation emitted by the blackbody. The formula is given by [51]:

$$\lambda T = k = 2.8978 \times 10^6 \, K.nm \,, \tag{2.47}$$

where λ is the wavelength of maximum emission in nm and T is the temperature of the object in Kelvin.

One can find the temperature of a star from its blackbody spectrum by treating it as a blackbody. For instance, the temperature of the Sun is found by assuming that its emission maxima is at 560 nm which is nearly equal to the response maxima of human eye. From this information, we can find the Sun's surface temperature as $T = 5174$ K. In our studies, λ_{max} of each spectrum was measured to determine the color temperature from Wien's Law.

2.7. Color Analysis of One of the Erbium-Doped Copolymer Samples

We explain the use of the above formulations by performing the color analysis of one of the erbium-doped copolymer samples in detail. The sample is 5 weight % erbium trichloride hexahydrate ($ErCl_3.6H_2O$) doped elastomeric poly (ether-urethaneurea) copolymer (PUU). This sample contains 2.19 % by weight trivalent erbium ions. We introduce this sample because of its closest colorimetric parameters.

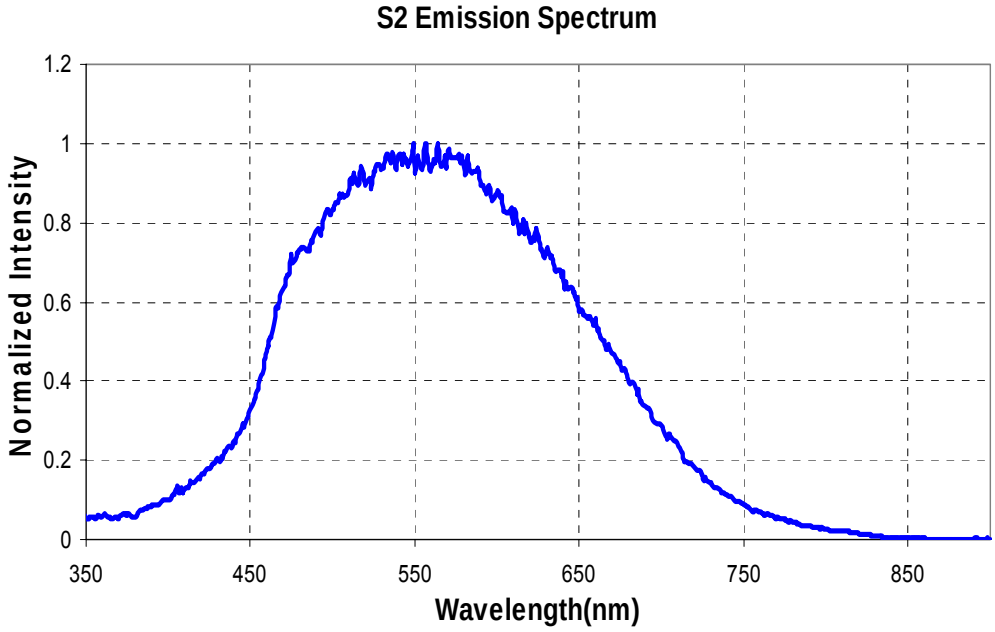

Figure 2.6: The emission spectrum of S2 (doped with 2.19% by weight erbium ions).

From this emission spectrum of 2.19 weight % erbium-doped polymer sample, we can obtain all of colorimetric calculations. We first calculate the tristimulus values and compare them with those for the D65 daylight source. The results are displayed in Table 2.2.

Tristimulus values	**Self-luminescence of D65**
$\mathbf{X_n}$	94,81106006
$\mathbf{Y_n}$	100
$\mathbf{Z_n}$	107,3046695
	Self-luminescence of S2 sample
X	87,85802511
Y	100
Z	45,16066088

Table 2.2: The tristimulus values of self-luminescence of D65 and S2 sample (2.19 weight % erbium-doped).

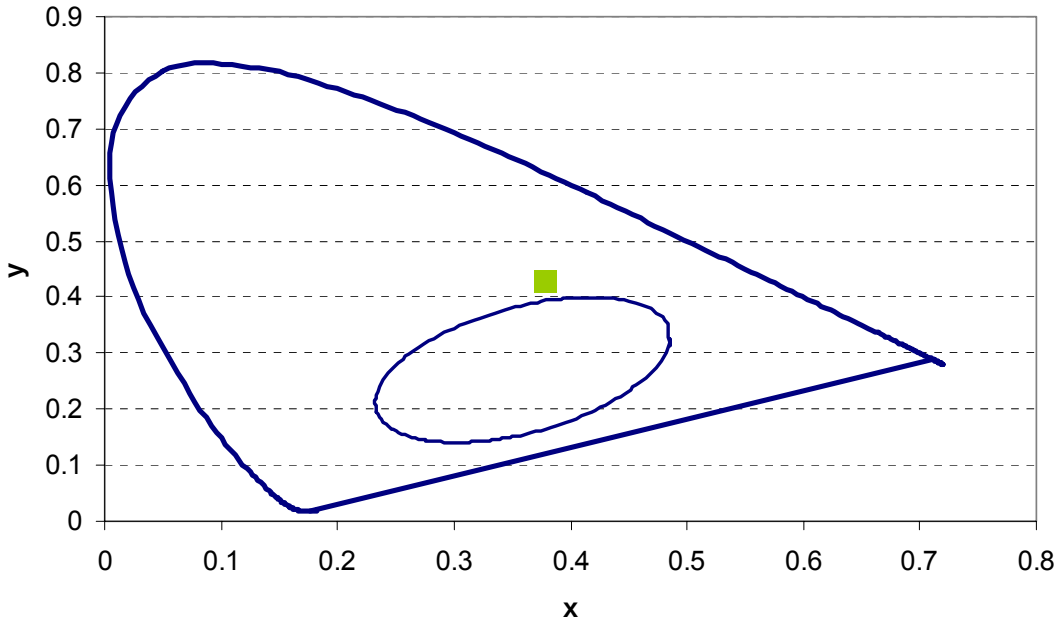

Figure 2.7: The (x, y) coordinates of the erbium-doped S2 sample (2.19 % by weight).

These results of tristimulus values are found by using equations (2.21), (2.22), (2.23) and (2.24). These are for the self-luminous tristimulus values which do not contain the $\beta(\lambda)$ factor because of self-luminosity. (x, y) coordinates of the sample are found from equations (2.25) and (2.26) which are for self-luminescence of our sample. We do not use the tristimulus values of object-color stimulus because there are eight $\beta(\lambda)$ factors and we could not specify any of them to use for (x, y) color coordinates. The (x,y) coordinate of our sample which takes the value (0.38, 0.43) could be seen in the figure below. Moreover, an example of (x, y) point is seen in Figure 2.7 for 2.19 % by weight erbium-doped polymer sample. This point suggests the closeness of our (x, y) coordinate to the ellipsoidal white region of the color chart.

Afterwards, the calculated tristimulus values of object-color stimulus are displayed in Table 2.3. Equations (2.38) and (2.39) are used for these calculations. These values are found for eight test-color samples which will be used in L*, a*, and b* calculations.

Tristimulus values	**1st sample for D65**
Xn	31,88410926
Yn	28,87107376
Zn	23,93435918
	1st sample for S2 sample
X	31,66360724
Y	30,23377856
Z	10,22702581

Table 2.3: The tristimulus values of object-color stimulus for the first test-color sample.

When we implement these results into L*, a* and b* formulas (Equations (2.35), (2.36) and (2.37)), we obtain the values shown in Table 2.3.

	For S2 sample
L*	61.85541043
a*	20.23576081
b*	12.32711015
	For reference sample
L_0*	60.66767643
a_0*	17.23887368
b_0*	10.89395644

Table 2.4: L*, a*, b* and L_0*, a_0*, b_0* coordinates with the implementation of X, Y, Z values.

Once these coordinates are determined, we reach the color difference and R_1 results. These parameters are calculated with the help of equations (2.42), (2.43) and (2.44).

ΔE_1	3,527885214
R_1	83,77172801
CRI	70

Table 2.5: Parameters for obtaining CRI of sample S2 which is doped with 2.19 weight % Er^{3+}

Final value of color rendering index is attained with the implementation of various formulas which are Equations in the range of (2.35)-(2.44). Note that color rendering index represents the quality of rendition of all colors equally which are radiated from the light source.

Then, the eye overlap index calculations give the eye overlap index (η) which describes the resemblance degree of our spectra with the eye response. That property gives the degree of whiteness of our light source. The comparison graph of the sample S2 (2.19 % by weight erbium-doped) and the response for the eye is shown in Figure 2.8. For this particular case, the η factor is determined to be 0.88, which is so close to 1. From the peak wavelength of the emission spectrum, we also obtain the color temperature of the light source to be 5138 K.

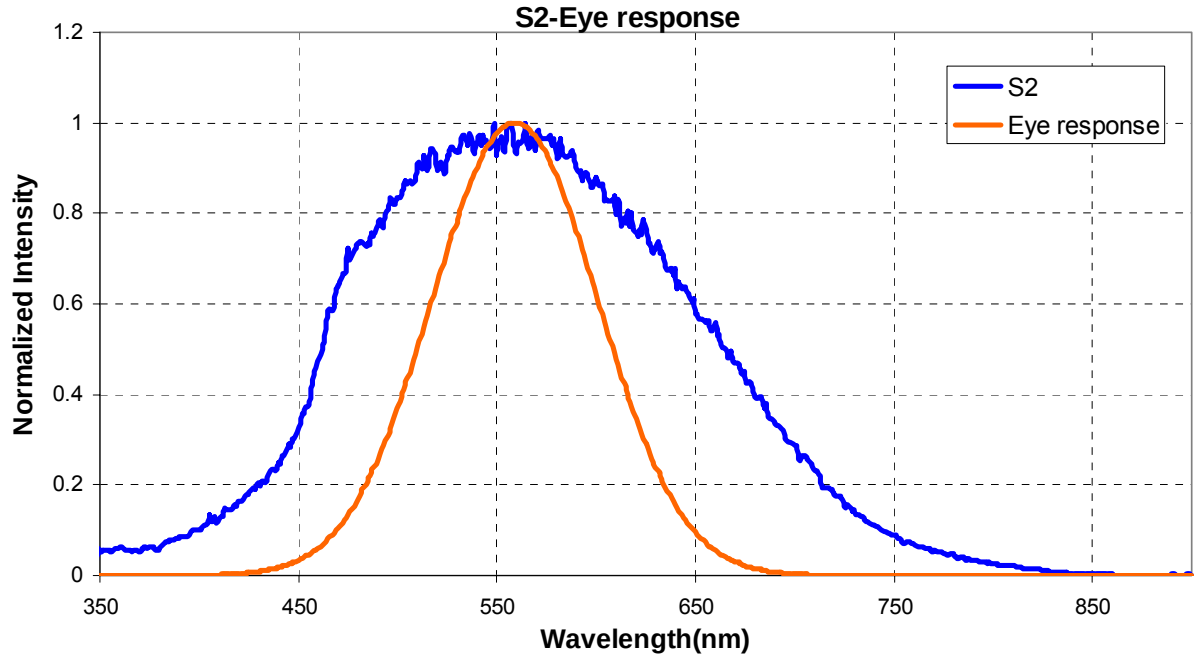

Figure 2.8: Eye response spectrum and the emission spectrum of sample S2 which is doped with 2.19% Er^{3+}.

In conclusion, in order to explain the general meaning of color perception, we have described some elements of visual system of a human. We then described the standard methods used in color analysis and discussed the calculation of tristimulus values, (x,y) coordinates, color-rendering index, eye-overlap factor, and color temperature. As a specific example, we performed the color analysis of a 5 % erbium trichloride hexahydrate ($ErCl_3.6H_2O$) doped sample which contains 2.19 % Er^{3+}.

Chapter 3

EXPERIMENTAL SETUP AND MEASUREMENTS

In order to obtain broadband UV-VIS converters, we used segmented thermoplastic poly(ether-urethaneurea) (TPUU) copolymer films. TPUUs have wide application areas, for instance; in the production of textile fibers, adhesives, protective coatings, membranes, and biomaterials. The widespread usage is the result of commercial availability of starting materials for their synthesis and their flexible polymerization techniques [52, 53]. In this chapter, we first describe the synthesis of poly(ether-urethaneurea) copolymers. Then, the doping process with erbium trichloride hexahydrate ($ErCl_3.6H_2O$) is briefly described. Afterwards, the setups for absorption and emission spectrometers are discussed. Also, the main features of these spectrometers are explained.

3.1.1. Synthesis of Poly (ether-urethaneurea) (PUU) Copolymer

Polymerization reactions were carried out at room temperature, in a 3-neck, round-bottom Pyrex flask equipped with an overhead stirrer, nitrogen inlet and an addition funnel. Poly(tetramethylene oxide)glycol oligomer (PTMO–2000) (15.700 g, 7.696 mmol) and 4,4'-diphenylmethane diisocyanate (MDI) (3.850 g, 15.390 mmol) were introduced into the reactor and dissolved in 28.2 g of dimethylformamide (DMF). Prepolymer formation was performed in 30 minutes. 0.138 g water was blended with 15.8 g DMF which was introduced into the addition funnel and added into the reactor slowly in about 2 hours. As the viscosity increased the reaction mixture was diluted with 66.0 g DMF.

As provided in the chemical structure below, in Figure 3.1. again, the poly(etherurethane-urea) consists of alternating soft (polyether) and hard (urethaneurea) segments along the polymer backbone. The chemical structure of the water chain-extended TPUU copolymer used in this study had 20.2% by weight hard segment.

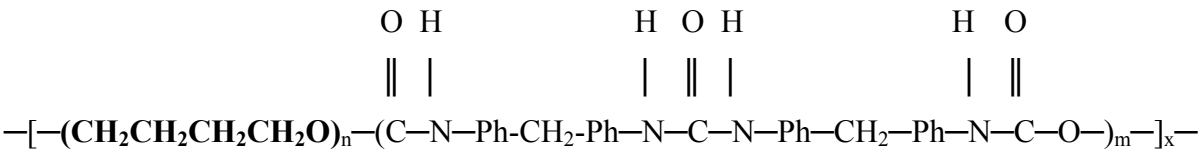

Figure 1.3: Chemical structure of poly(etherurethane-urea).

In this structure, bold symbols represent the polyether soft segment, which has a number average molecular weight of 2040 g/mol. From the stoichiometric calculations, the urethaneurea hard segment has a number average molecular weight of about 505 g/mol.

3.1.2. Preparation of Erbium-Doped Polyurethaneureas

Depending on the level of doping, calculated amount of $ErCl_3.6H_2O$ was dissolved in DMF to produce a dilute solution containing about 10% by weight of dopant. Solution was sonicated for 5 minutes at room temperature to obtain complete dissolution. $ErCl_3.6H_2O$ solution was then mixed with the polymer solution and further sonicated for 5 more minutes. Clear solution obtained was poured into a Teflon mold and solvent was evaporated in an air oven at 60 °C, overnight. Complete removal of DMF was obtained in a vacuum oven at 60 °C, until constant weight is achieved. Table 4.1 gives a list of the $ErCl_3.6H_2O$ doped TPUU samples prepared and their compositions.

3.2. Absorbance Measurements

We performed absorption spectroscopy experiments to observe the absorption bands. These measurements were done on a Schimadzu UV-VIS-NIR spectrophotometer which is shown in Figure 3.2 (3101 PC model). In absorption spectroscopy, the light is sent through our sample. Some amount of light is transmitted, some is absorbed. The value of the absorbance is found from incident and transmitted intensities of light. The absorbance is represented as

$$A = \log \frac{I_0}{I_t} \quad . \tag{3.1}$$

In this formula, I_0 is the intensity of the incident beam and I_t is the intensity of the transmitted beam. The logarithm of the intensity ratio is in the base of 10. The value of the absorbance depends on the wavelength of the incident beam of light and the absorbance spectrum is drawn by the help of this formula. The wavelength of the absorbance peaks represents the required energy for the electron to be excited to higher levels. It means that the absorbance is not the same for all wavelengths. The aim of the absorption spectrum is to see and analyze the peaks of the absorbance.

We obtained the spectrum in the UV-VIS region. For all experiments, the used parameters are medium scan speed, scan step in 1 nm interval and wavelength resolution in 1 nm through the range of 300-3200 nm. The spectrometer is seen in Figure 3.2:

Figure 3.2: Schimadzu spectrophotometer for taking absorbance measurements.

In Figure 3.3, the absorption spectrum of S2 which is 2.19% Er^{3+}-doped sample is seen. It has absorption bands around 380 nm ($^4G_{11/2} \rightarrow {}^4I_{15/2}$), 430 nm ($^4F_{5/2} + {}^2H_{9/2} \rightarrow {}^4I_{15/2}$), 490

nm ($^4F_{7/2} \rightarrow {}^4I_{15/2}$), 520 nm ($^2H_{11/2} \rightarrow {}^4I_{15/2}$), and 650 nm ($^4F_{9/2} \rightarrow {}^4I_{15/2}$). The samples were excited in the absorption band of the host materials. Excitation was obtained by using a pulsed, tripled Nd:YAG laser at 355 nm.

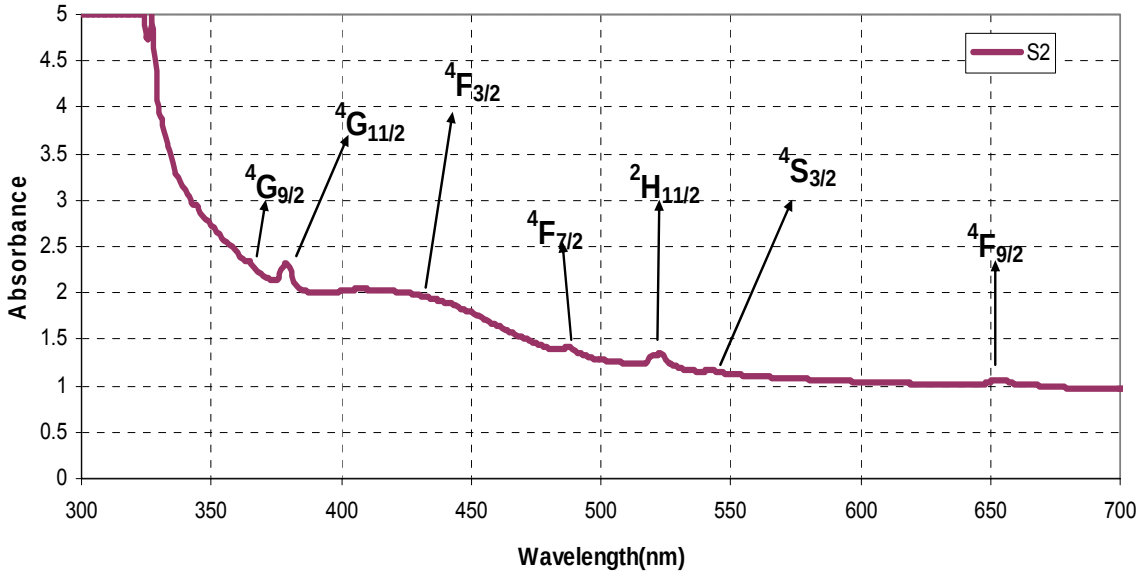

Figure 3.3: Absorption spectrum example for S2 (2.19 weight % Er^{3+}-doped copolymer) sample.

3.3 Photoluminescence Measurements

Photoluminescence measurements were done with the help of the PL spectrometer which is seen in Figure 3.4. We used 1064 nm Nd: YAG laser to obtain 355 nm to excite the samples in UV region.

In order to obtain doubling of frequency, 10 mm long potassium titanyl phosphate crystal (KTP) was used. There were two kinds of wavelengths which were fundamental (1064 nm) and second harmonic (532 nm) beams inside the 20 mm long lithium triborate crystal (LBO). In LBO crystal, there existed three-wave mixing process to obtain 355 nm light. After passing it, we had three kinds of wavelengths; 1064 nm, 532 nm and 355 nm. Then, we used a band-pass filter (F27) to prevent the passage of wavelengths other than 355 nm.

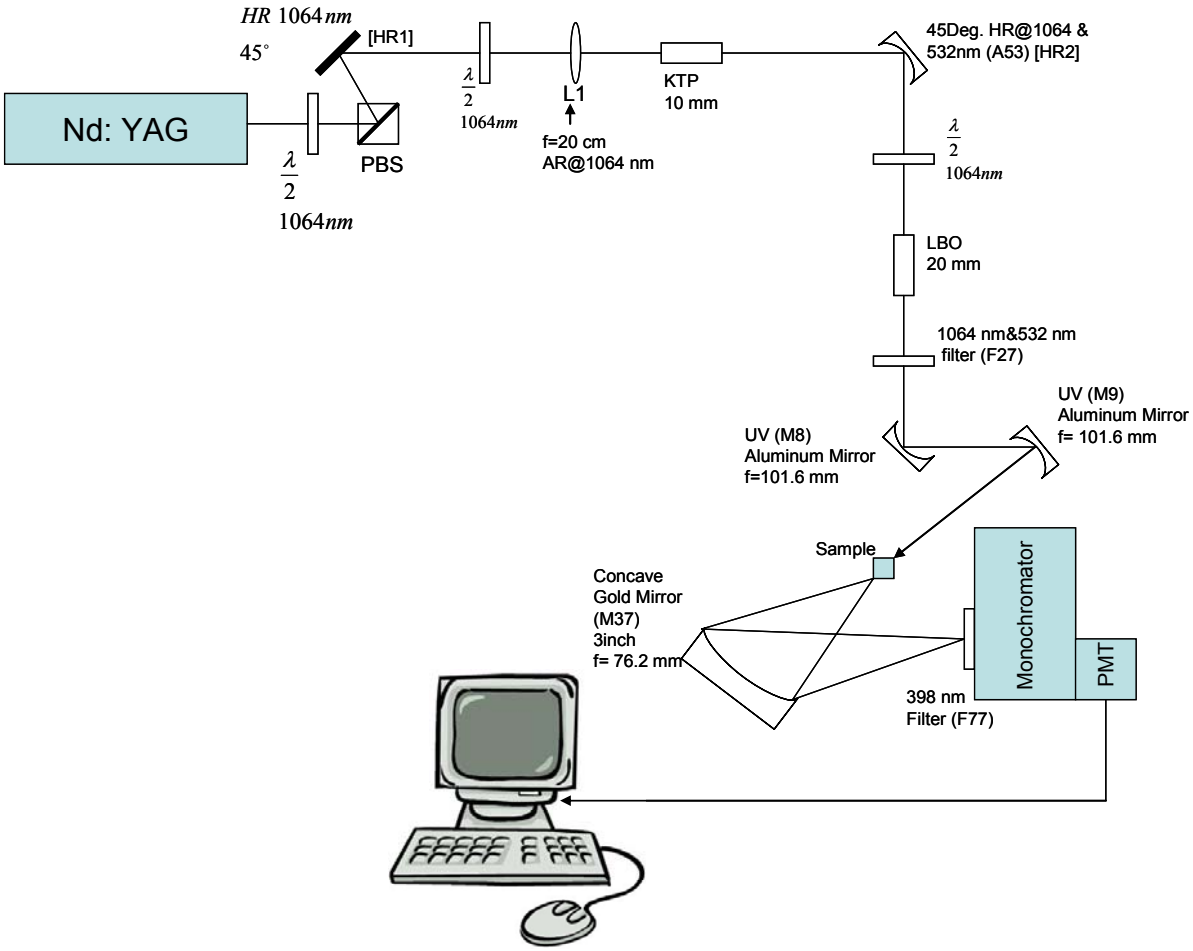

Figure 3.4: Schematic of the setup used for emission spectrum measurements.

In these PL measurements, Nd:YAG power was 0.95 W after the lens L1 and incident UV pump power was 14 mW after the M9 mirror. The pump beam was focused onto the polymer sample from the curved aluminum mirror (M9). Then, the fluorescence emitted from the sample was gathered with the concave gold mirror. Before the monochromator, there was F77 filter to prevent the entry of UV pump beam. The slit of the entrance of the monochromator was around 0.5 mm. We used the CVI, DK 4800 model emission spectrometer as monochromator.

A monochromator selects single spectral line or a narrow band from a wider portion of the spectrum. It is used to produce monochromatic light. Upon reflecting through the collimating mirror, the light is diffracted into different wavelengths with diffraction grating

which is used as dispersion element. The diffraction takes place at various angles. The monochromator is adjusted to select one specific narrow band by arranging the position of the grating.

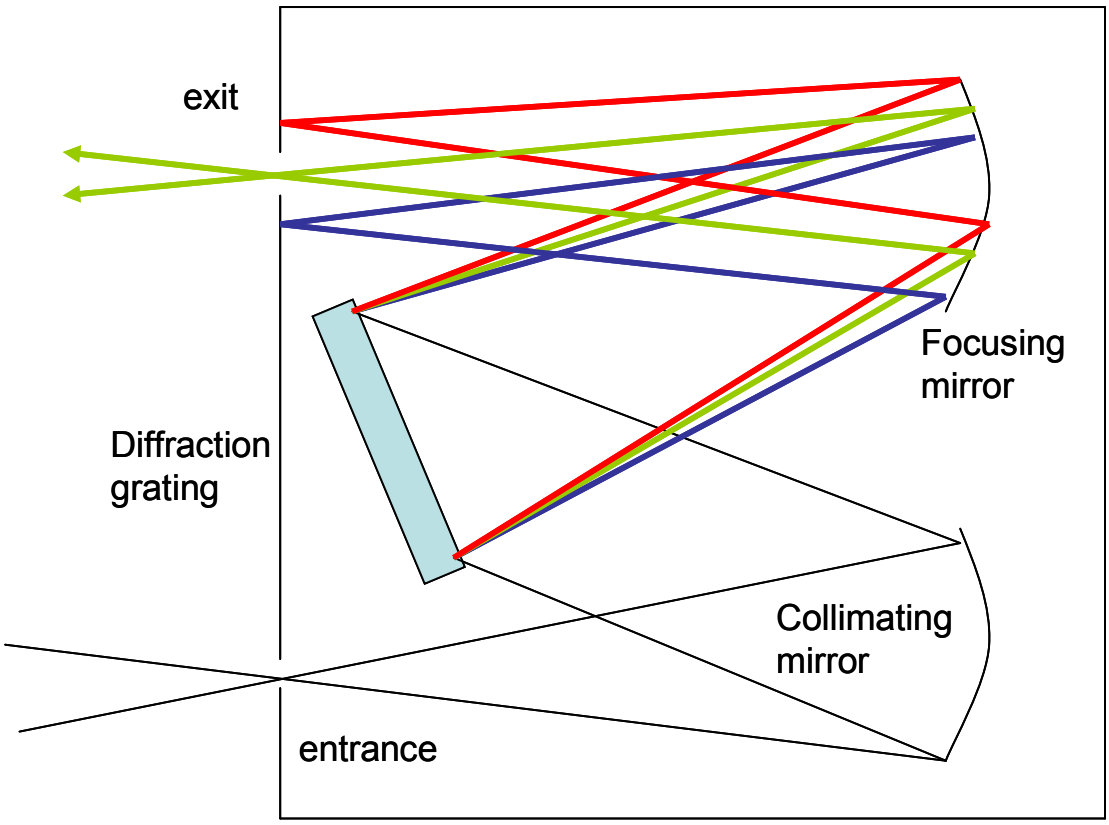

Figure 3.5: The representation of Czerny-Turner monochromator optical pathway.

In Figure 3.5, one can see the green selection of the Czerny-Turner type monochromator. The other light rays can be chosen by the adjustment of diffraction grating. In Figure 3.5 the incoming light is a beam of polychromatic light.

After the monochromator, there was an optical detector which was Photomultiplier Tube (PMT) in our case. PMT detects the light in order to convert it into an electrical signal. Photomultiplier tube (PMT) is a widely used light detector which performs in near ultraviolet, visible, and near infrared regions of electromagnetic spectrum. The benefit of PMT is that it is very sensitive to low levels of light intensity [54]. There is a photocathode and a number of dynodes inside a vacuum enclosure which is seen in Figure 3.6.

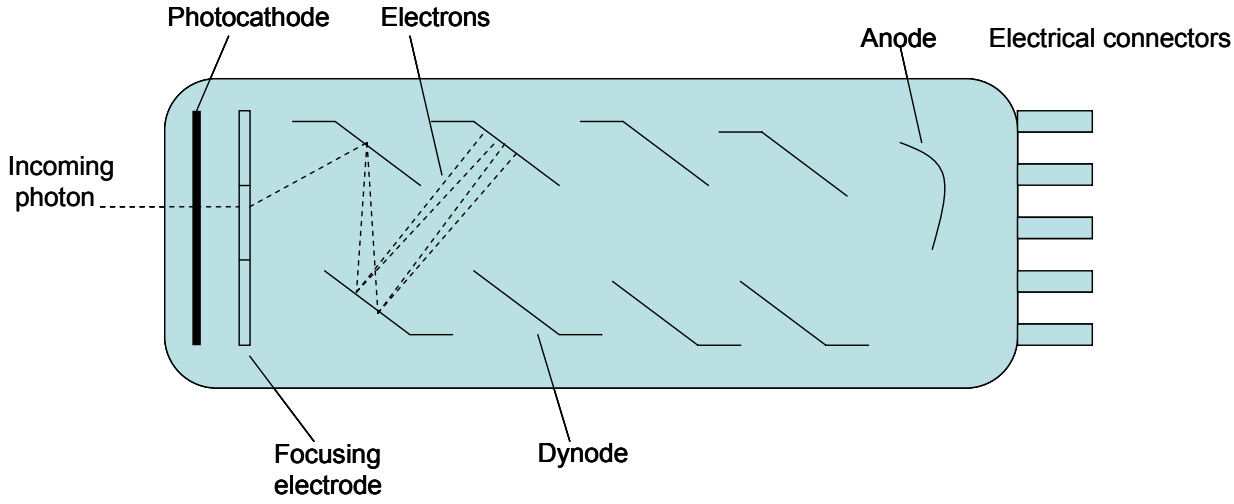

Figure 3.6: The configuration of a Photomultiplier Tube.

The vacuum is for preventing the collisions of electrons with gas molecules [54]. A photon impinges upon the photocathode and produces a photoelectron suitable with the photoelectric effect. According to the photoelectric effect, there is a specific work function for each surface in order to break off the electrons from it by the help of striking photon. The photocathode involves materials which have low work functions to separate the electrons easily [54]. There are a series of electrodes called dynodes through which the photoelectron is accelerated. The photocathode can take a high negative voltage value in between -500V and -1500V. The dynodes are deposited with less negative potentials, consecutively. In Figure 3.6 there is an anode which is the last electrode in order to gather the photoelectrons. The electrons break off the photocathode with the incident photon energy. When they are transferred through the second dynode, they are accelerated by the electric field to have a larger energy. The number of photoelectrons increases at each dynode. Then, the anode takes the collection of electrons and results in a sharp pulse to express the incoming photon to the photocathode.

Our PMT was operated at the voltage of -800 V. Both of the entrance and exit slit widths of the monochromator were 200 μm. We used the grating which is in the range of 330-1500 nm. Before taking the emission spectral result of our sample, we adjusted the

position of the sample to maximize the signal that was seen in the oscilloscope. In Figure 2.6, there is an example of emission spectrum for 2.19 weight % Er^{3+} doped polyurethanes.

In the next chapter, the final absorption-emission spectra will be presented and the evaluation of these results will be discussed. The colorimetric results which are CRI, color coordinates, and eye overlap factor will be determined as described in Chapter 2. General interpretation for the colorimetric parameters will be done.

Chapter 4

RESULTS AND DISCUSSION

In this research, thermoplastic poly(ether-urethaneurea) (TPUU) copolymers containing aromatic diisocyanate (MDI) and poly (tetramethylene oxide) soft segments were prepared. The polymers were doped with erbium trichloride hexahydrate ($ErCl_3.6H_2O$) in varying concentrations (5 to 25 weight %) and we obtained final polymer films after evaporating the solvent. As it can be seen in Table 4.1, the resulting polymers had Er^{3+} contents between 2.19 to 10.86% by weight. The preparation procedure was briefly explained in Chapter 3.

In this chapter, we first present the results of the absorption and emission measurements. Then, the results of the colorimetric analysis will be discussed. This will be followed by general discussion and conclusions. In Table 4.1, amount of erbium trichloride hexahydrate ($ErCl_3.6H_2O$) in each sample and the corresponding trivalent erbium ion concentration (in weight %) are listed. In that table, final values of color coordinates, color rendering indices, and eye overlap factors are also indicated.

Sample Code	$ErCl_3.6H_2O$ (wt%)	Er^{3+} (wt%)	**x**	**Y**	**CRI**	**T_C(K)**	**η**
S1	0	0	0.29	0.41	61	5540	0.85
S2	5.00	2.19	0.38	0.43	70	5138	0.88
S3	9.64	4.22	0.38	0.44	68	5175	0.89
S4	14.82	6.49	0.42	0.48	58	5212	0.92
S5	24.78	10.86	0.41	0.47	57	5093	0.95

Table 4.1: Weight % values of $ErCl_3.6H_2O$ and Er^{3+}, color coordinates (x, y), color rendering index (CRI), color temperature (T_C), and eye overlap factor (η) of the undoped and erbium doped samples. Color coordinates and CRI values were evaluated by using the CIE 1964 standards.

4.1: Experimental Investigations

In the experimental part of the study, absorption and photoluminescence measurements were performed. Absorption spectroscopy was conducted to observe absorption bands. These experiments were carried out with a Schimadzu UV-VIS-NIR spectrophotometer. The setup of absorption spectrophotometer is provided in Figure 3.2. Moreover, photoluminescence measurements were made by using the photoluminescence (PL) spectrometer. 1064 nm Nd: YAG laser was used to obtain 355 nm excitation wavelength. The setup of the PL spectrometer can be seen in Figure 3.4.

4.1.1: Absorption Measurements

In Figure 4.1, the absorption spectra of the undoped and 6.49% erbium doped sample are shown. In the doped sample, the typical absorption lines of Er^{3+} which are around 380 nm ($^4G_{11/2} \rightarrow {}^4I_{15/2}$), 430 nm ($^4F_{5/2}+{}^2H_{9/2} \rightarrow {}^4I_{15/2}$), 490 nm ($^4F_{7/2} \rightarrow {}^4I_{15/2}$), 520 nm ($^2H_{11/2} \rightarrow {}^4I_{15/2}$), and 650 nm ($^4F_{9/2} \rightarrow {}^4I_{15/2}$) are seen. Furthermore, the other two absorption lines (364 nm ($^4G_{9/2} \rightarrow {}^4I_{15/2}$) and 542 nm ($^4S_{3/2} \rightarrow {}^4I_{15/2}$)) are weak but still visible.

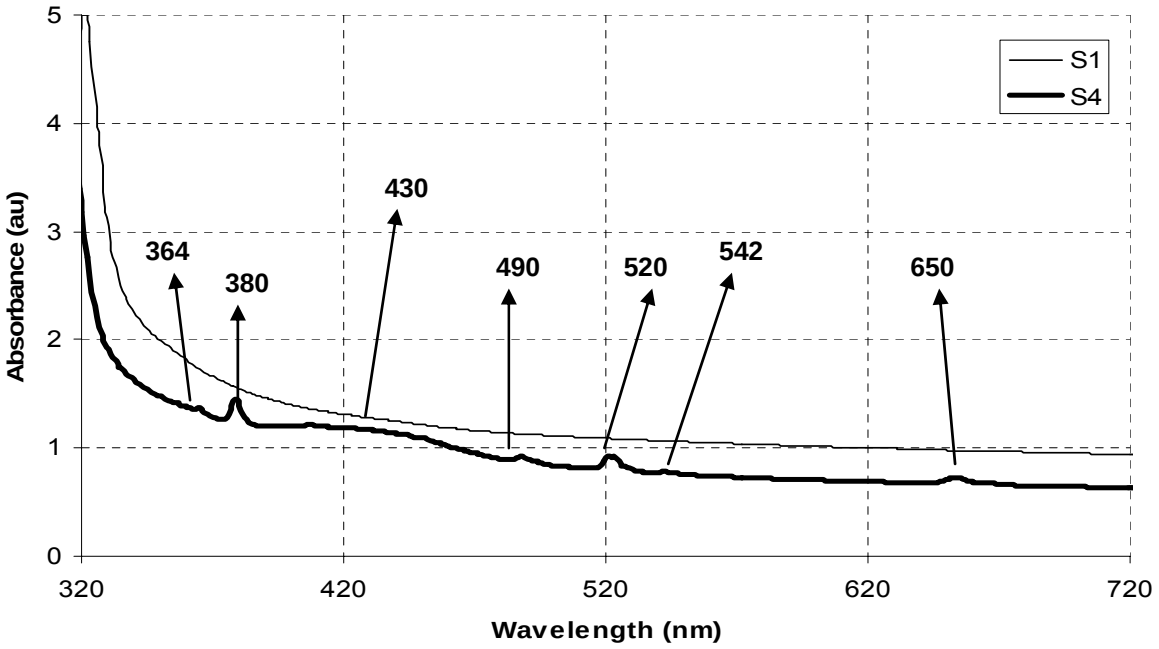

Figure 4.1: Absorption spectra of S1 (undoped) and S4 (649 % Er^{3+} doped) samples. The visible absorption bands of trivalent erbium ion can be seen in the spectrum of S4.

4.1.2: Emission Measurements

We excited the samples in the absorption band of the polymer host by using the triple harmonic of the Nd:YAG laser at 355 nm. We analyzed the emission spectra of our samples as a function of their Er^{3+} concentration. The emission spectra of S1 and S4 (undoped and 6.49 % Er^{3+} doped samples) are shown in Figure 4.2. The undoped sample has the emission spectrum in the blue-green portion of the electromagnetic spectrum. For the trivalent erbium doped sample, the spectrum shifts to the red region. In this case, the spectrum extends from 400 to 750 nm and covers the entire visible spectrum. In order to obtain UV-VIS converters, one needs a material that emits with a broad spectrum in the range of 400-750 nm.

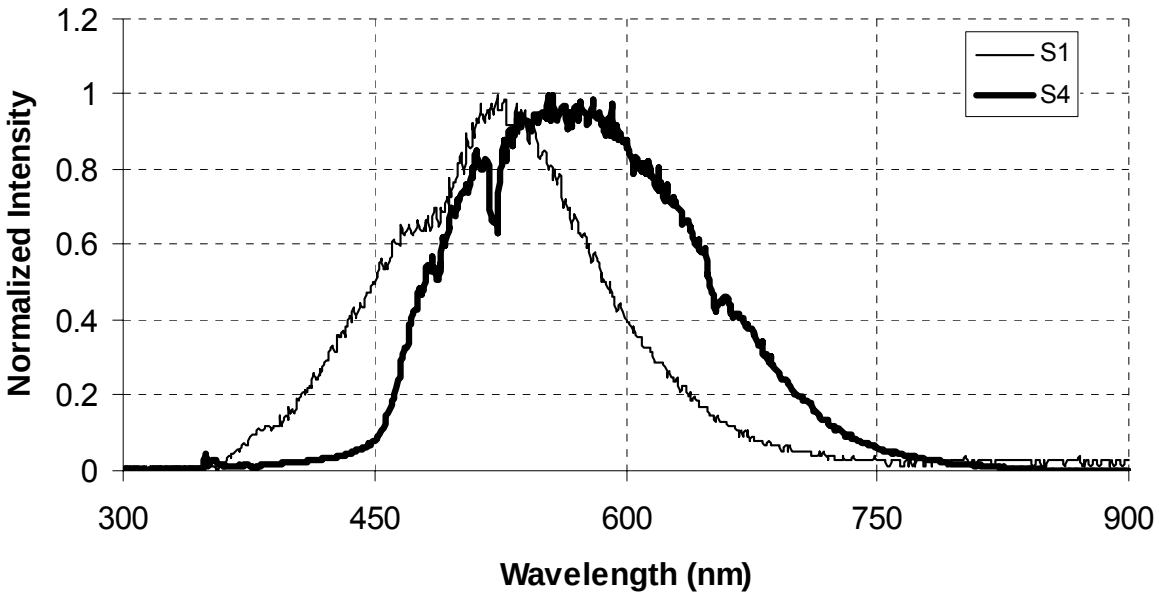

Figure 4.2: Emission bands of S1 and S4 samples. The doped one has the spectrum which is shifted to the red region of the electromagnetic spectrum.

4.2: Colorimetric Results

The colorimetric results which are color coordinates, color rendering index (CRI), color temperature (T_C), and overlap factor (η) are seen in Table 4.1. These were found by the help of 1964 CIE standards. These CIE standards contain color-matching functions which are used to identify the final vision. The colorimetric outcomes were found by the help of color-

matching functions and chromaticity coordinates. The calculation techniques of colorimetric parameters were explained in Chapter 2.

4.2.1: Color Coordinates (x, y)

In Figure 4.3, the color coordinates of each sample are shown inside the color chart. These coordinates are not inside but very close to the white region of the color chart. For the sample S2 with 2.19 % erbium by weight, color coordinates become closest to the white region. The results indicate that at low erbium concentrations, increase in the erbium concentration brings the emission closer to the white region. However, for high weight percentages, the emission spectra move further away from the white region. We believe that this is due to the self-absorption of trivalent erbium ion at high doping concentrations, results the distortion of the emission spectrum.

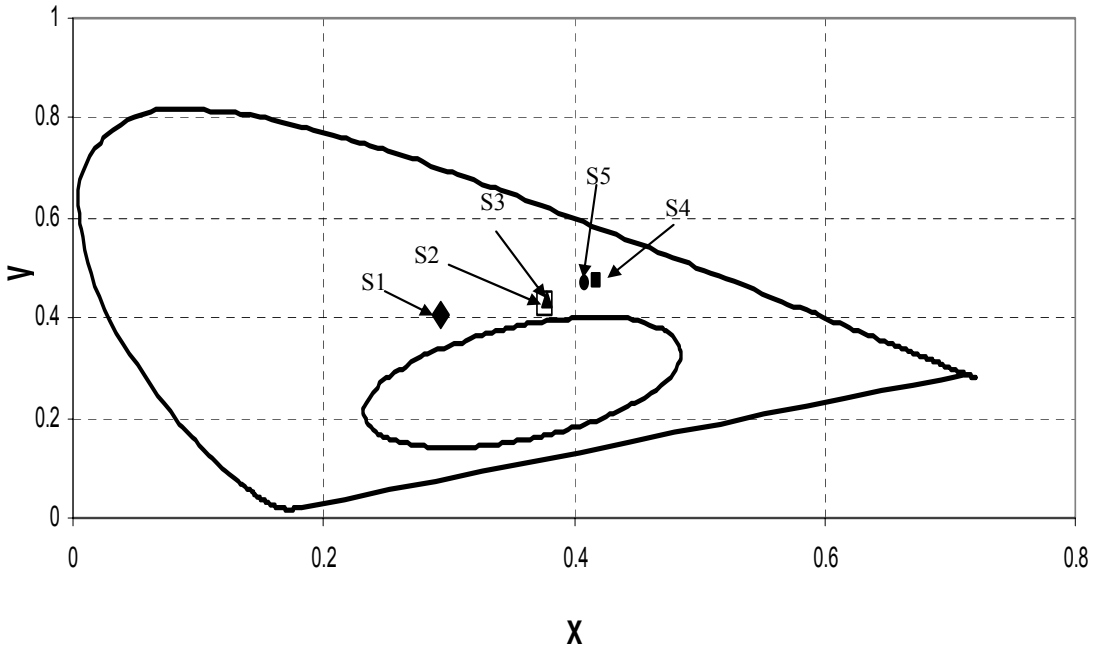

Figure 4.3: CIE color chart which indicates the color coordinates of each trivalent erbium doped polymer sample. The proximity to the white region of the color chart shows the quality of whiteness of the light sources. S1, S2, S3, S4, S5 representations refer to undoped, 2.19%, 4.22%, 6.49%, and 10.86% Er^{3+} doped polymer samples, respectively.

These results indicate that there is an optimum concentration of erbium ions which brings the (x, y) coordinates closer to the white region of the color chart.

4.2.2: Color Rendering Index (CRI)

In Figure 4.4, there are two spectra of S2 and S5 samples which have 2.19 and 10.86 weight % Er^{3+} respectively in order to exhibit the effect of the dopant concentration on the photoluminescence spectrum. In S5 polymer sample, the self absorption of the erbium ions can be seen evidently at 523 nm. It originates from the excess of ion concentration and then the color coordinates move away from the white region of the color chart. Furthermore, color rendering index (CRI) is also influenced by the dopant concentration. As shown in Table 4.1, for doping of 2.19% by weight, CRI value increases to 70. However, for the doping concentrations higher than 2.19%, the CRI value decreases down to 57. We can see the closeness of CRI values of erbium doped samples when we compare with previous studies on the investigation of whiteness. For instance, CRI value is 71 for CdSe/ZnS quantum dots which are hybridized with InGaN/GaN LEDs [4].

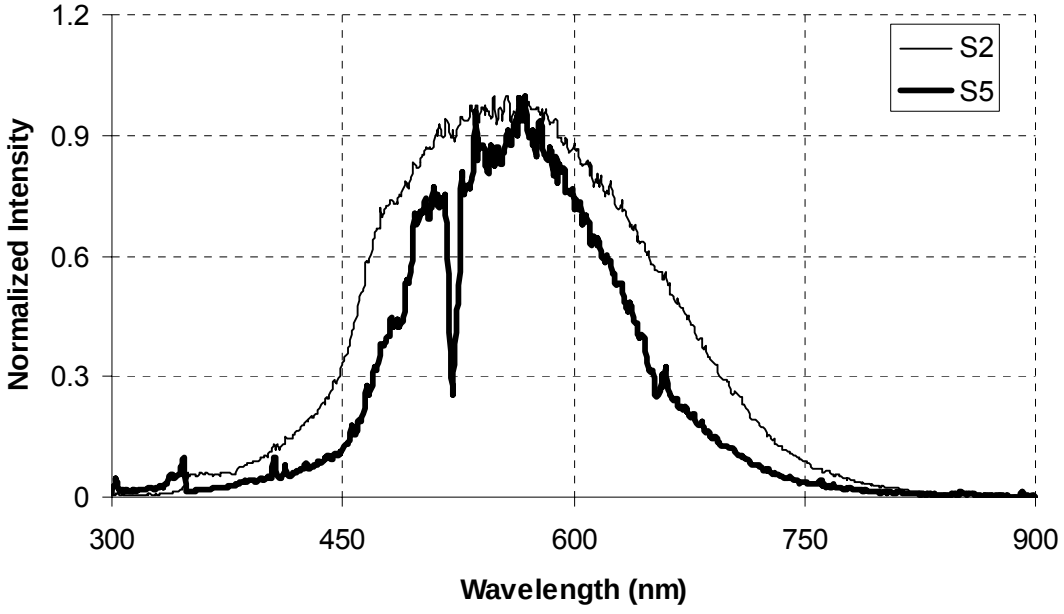

Figure 4.4: Emission spectrum of S2 (2.19 weight % doped) and S5 (10.86 weight % doped) polymer samples. In the spectrum of S5, self absorption can be seen nearly around 523 nm.

Furthermore, in luminescent semiconducting polymers which are blended with organometallic emitters, the value of CRI becomes 86 and 92 for two different types of devices [16].

4.2.3: Color Temperature (T_C)

Color temperature (T_C) of a light source indicates the color scale of white light compared to a blackbody radiator. For illumination applications, T_C should be in between 3000 and 7500 K [16]. The reported values are different for various emitters such as 6400 K and 4600 K for two different types of semiconducting polymers which are blended with organometallic emitters [16]. Furthermore, the value of 4500 K was found for ZnSe thin films –grown by atomic layer deposition (ALD) which is an operation to form thin coatings- which are excited by an electron beam [17]. The reported T_C values for our case, as can be seen in Table 4.1, are in the range of 5093-5540 K.

4.2.4: Eye Overlap Factor (η)

In Figure 4.5, the emission spectrum of the S4 sample together with the spectral response curve for the eye can be seen. The emission band of S4 covers the visible portion of the spectrum entirely. Furthermore, the emission band extends through the outside of the visible spectrum. In order to determine the degree of overlap between the emission spectrum of the samples and the eye response curve, we introduced an overlap factor η, defined by

$$\eta = \frac{\int_0^\infty I_s(\lambda) R_e(\lambda) d\lambda}{\sqrt{\int_0^\infty I_s^2(\lambda) d\lambda} \sqrt{\int_0^\infty R_e^2(\lambda) d\lambda}} \tag{4.1}$$

In this equation, $I_s(\lambda)$ is the spectral intensity distribution of the sample, $R_e(\lambda)$ is the spectral response of the eye and λ is the wavelength. When these two values are equal, η becomes "1". The value of η increases from 85% to 95% as the concentration of erbium is increased from 0 to 10.86% by weight. The change in η is caused by the self absorption bands of erbium around 490, 523, and 660 nm which are shown in Figure 4.5. As a result, the

emission band becomes narrower and the overlap takes better value in comparison with samples containing lower level of erbium.

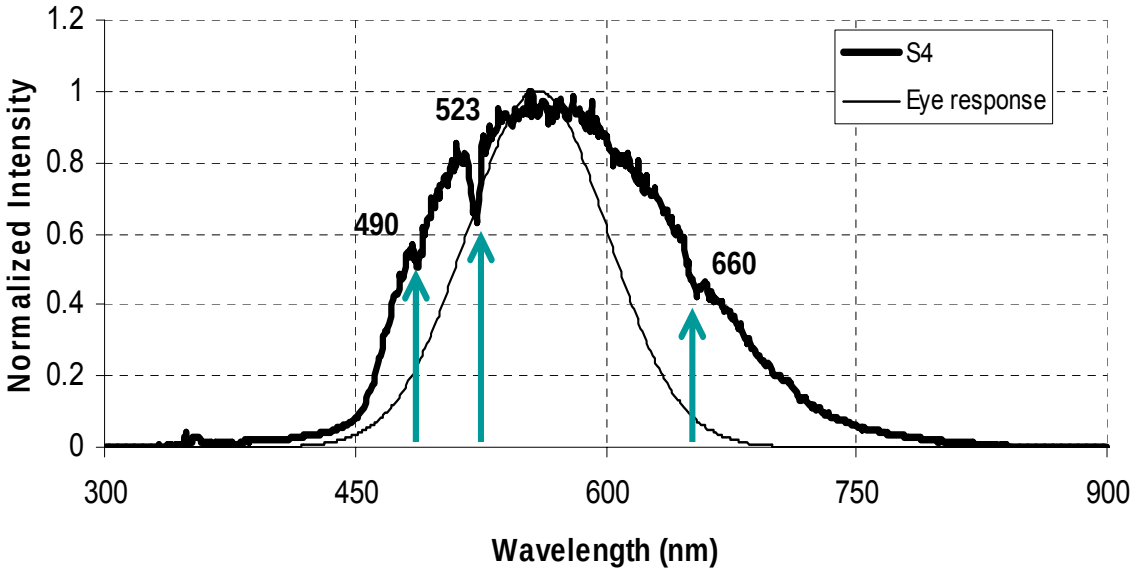

Figure 4.5: The emission spectrum of S4 (doped with 6.49% erbium ion) with the response curve for the eye.

Chapter 5

CONVERSION EFFICIENCIES OF ERBIUM-DOPED POLYMERS

In this chapter, we investigated the conversion efficiencies of the samples. Conversion efficiency gives the ratio of incident power that is converted to fluorescence power. In order to determine the efficiency values, we established a new setup which is shown in Figure 5.1.

By the help of this new setup, we aimed to generate UV pump light at 355 nm in order to measure the conversion efficiencies of each sample. There are two various nonlinear crystals to obtain 355 nm pump light as the only excitation wavelength which we used. One of them is the 10 mm long potassium titanyl phosphate crystal KTP and the other one is the 20 mm long lithium triborate crystal LBO. In KTP, we obtained 532 nm light with second harmonic generation. At first, there were two kinds of wavelengths which were fundamental (1064 nm) and second harmonic (532 nm) beams inside the LBO crystal. Then, there existed three-wave mixing process to obtain 355 nm light. Afterwards, we had three kinds of wavelengths; 1064 nm, 532 nm, and 355 nm. Subsequently, we used a band-pass filter (Filter-27) to prevent the passage of wavelengths other than 355 nm.

In these measurements, concerning all samples, average incident UV pump power was 14.3 mW after the lens, and average fluorescent power is 0.02 after the filters. The pump beam was focused onto the polymer sample from the lens L1 after the curved aluminum mirror (M9). Then, the fluorescence emitted from the sample was gathered with the CaF_2 lens which has 8 cm focal length. Filter-77 is for preventing the entry of UV pump beam, and Filter-66 is for selecting a band from the visible range.

In this setup, the laser light was focused into the polymer sample by putting a lens L1 with a focal length of 10 cm, and also the emitting light from the sample was collected by the CaF_2 lens with 8 cm focal length and 2.5 cm radius. In order to obtain maximal accumulation of fluorescent light, the sample and filters were displaced in the 2f-2f coordinates of the CaF_2 lens.

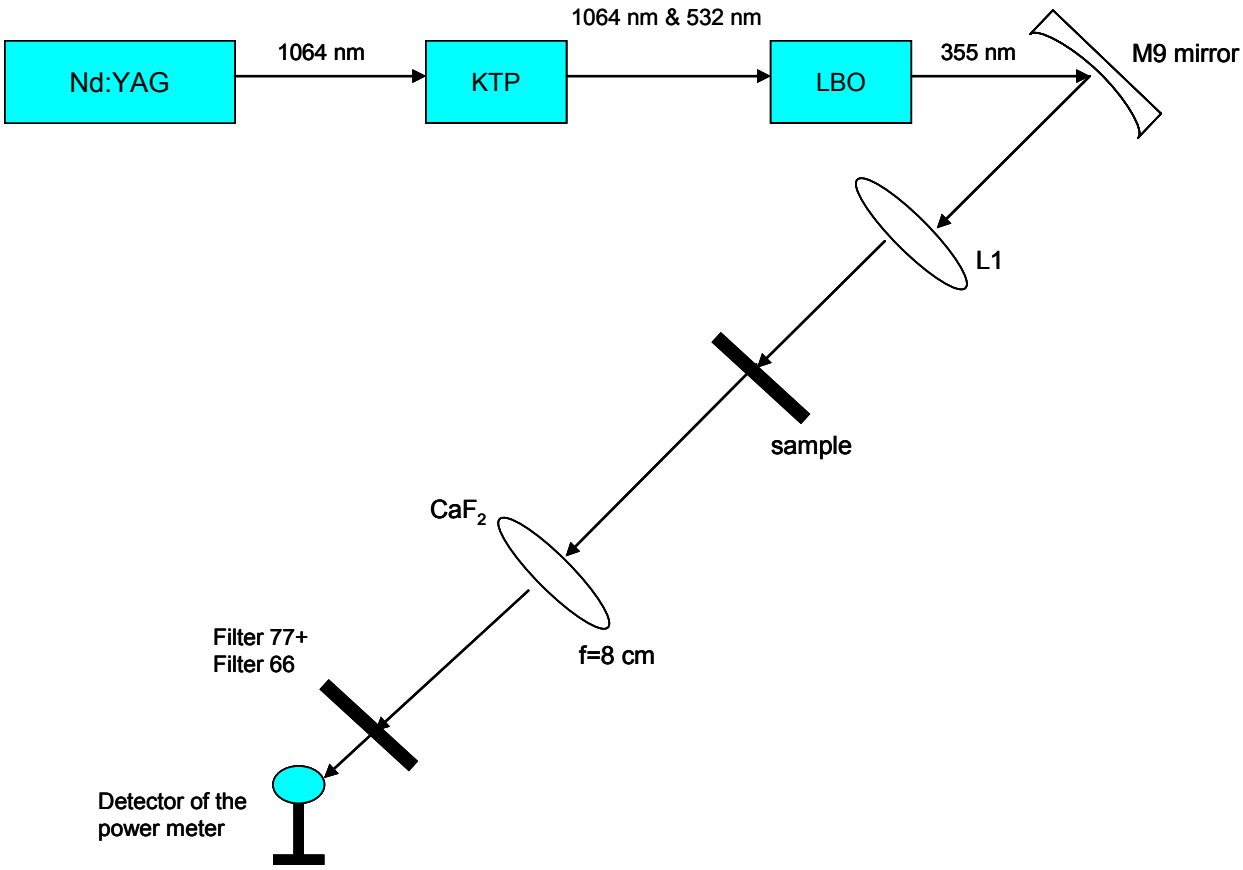

Figure 5.1: The setup used to measure the conversion efficiency of each sample

We used CaF_2 lens because it transmits UV light better. We placed a tube between filter and the detector of the power meter to prevent scattered light. Then, the silicon detector was calibrated to measure the power of fluorescence with high precision. Incident power was measured before the sample and fluorescent power was measured after the filters. Filter-77 is for preventing UV light and Filter-66 which has transmission around 330-630 nm is for selecting the visible range of the spectrum. The transmitted signal was in the range of 470 nm and 590 nm. We calculated the transmission after the sample by this formula below:

$$T = 10^{-A} \tag{5.1}$$

In this formula, A is the absorbance of the polymer sample. Absorbance is the unitless quantity which can be seen in Equation 5.2:

$$A = \log \frac{I_0}{I_T} \tag{5.2}$$

In that equation I_0 is the intensity of the incident light and I_T is the intensity of the transmitted light. As it can be known, $T = \frac{I_T}{I_0}$. We measured the transmission of the CaF_2 lens which has 8 cm focal length to be 0.89. There are two parameters which affect the value of the efficiency. These are Rayleigh scattering and Fresnel loss of the sample. At first, the concept of Rayleigh scattering will be described.

5.1. Rayleigh Scattering

Scattering is the emission of light by particles which are smaller than the wavelength of the incident light [55]. That is, it represents the separation of energy from an incoming light and following emission of some part of that energy [55]. As an example to Rayleigh scattering, the light ray of the Sun enters through the atmosphere from one way and it is scattered in all directions by the air molecules. If there were no atmosphere, we could not see the sky as blue. Rayleigh scattering dominates at high frequencies. By the aid of atmosphere, the blue or high-frequency part of the spectrum is scattered considerably while the red portion is not scattered, generally. Incident light scatters in all directions and it makes the whole sky as blue.

Lord Rayleigh investigated the frequency dependence of the scattered flux density. The scattered flux density is proportional to the fourth power of the driving frequency. It diminishes when the wavelength of the incident light increases as explained before. The transmitted intensity of light is represented as

$$I_T = I_i \exp(-\alpha_S z). \tag{5.3}$$

In this equation, I_T is the symbol of the transmitted intensity, I_i is incident intensity of light, 'α_S' is the scattering coefficient, and z is the thickness of the polymer. 'α_S' coefficient contains λ^{-4} dependence which can be seen in Equation 5.4:

$$\alpha_S = (2\pi)^4 (\lambda)^{-4} \frac{(n^2-1)^2}{6\pi N}. \tag{5.4}$$

In that equation, n is the refractive index of the material and N is the density of the atoms. We can express the relationship between scattering coefficient and differential scattering cross section with Equation 5.5:

$$\alpha_{S0} = \frac{\alpha_S}{\lambda^4} \tag{5.5}$$

In this equation, 'α_{S0}' is differential scattering cross section. In our research, we found final transmission from absorption spectrum measurements for the portions in which there are no Er3+ absorption bands. 'α_{S0}' coefficient was determined from the best-fit values of these transmission measurements. We used that approximation, because the value of the thickness may influence 'α_{S0}' scattering cross section in an incorrect way. $\frac{I_T}{I_i}$ gives T_S, transmission through sample (after scattering) removing the influence of Fresnel Loss. Upon subtracting transmission after scattering from "1", we can take mathematical value of the scattering loss:

$$L_S = 1 - T_S \tag{5.6}$$

In this equation, L_S is the scattering loss and T_S is the transmission through the sample. The scattered loss values at 355 nm wavelength which is the excitation wavelength of trivalent erbium-doped polymers are tabulated in Table 5.1. Average scattering loss is 0.95 for erbium-doped samples.

5.2. Fresnel Reflection Loss (L_F)

The other effective parameter to the transmitted intensity is Fresnel reflection loss. In illuminating objects, there is a reflected light back to the direction of the incoming light. That reflection is based on the refractive index difference between two media; erbium-doped polymer and air. This Fresnel reflection loss affects resulting transmission at each polymer surface. Some portion of the incoming light reflected back at both interface of the polymer sample which can be seen in that formula:

$$L_F = \left(\frac{n_1 - n_0}{n_1 + n_0} \right)^2 \tag{5.7}$$

The L_f ratio is the Fresnel reflection loss of the system, n_1 is the refractive index of our sample and n_0 is the refractive index of air. In our system, we found the refractive index of our samples with refractometer. We determined the approximate value for each one is 1.63. The refractive index of air is 1.0003 but [56], we obtained it as 1, roughly. In order to find the influence of Fresnel loss and Rayleigh scattering, we use Equation 5.8 which is seen below:

$$I_T = I_i (1 - L_F)^2 (1 - L_S) \tag{5.8}$$

That formula can also be represented with the values of transmissions:

$$T = T_F{}^2 T_S \tag{5.9}$$

Fresnel loss influences the transmitted intensity two times which are effective at two interfaces of the polymers. The determined Fresnel loss, L_F for our system is 0.06.

In order to find the result for the efficiency, the general efficiency formula can be written like that:

$$\eta_{eff} = \frac{P_{flour}}{P_{in}} \frac{\beta}{T_L} R \tag{5.10}$$

In that formula, P_{flour} is the fluorescence power of the system after the filters, P_{in} is the power inside the sample, β is the solid angle ratio, T_L is the transmission of the CaF_2 lens, and R is the spectral area ratio. As it was stated before, T was found as 0.89 for our system. The determination of the β, solid angle can be comprehended by the help of Figure 5.2. As it can be seen in this figure, the light goes from sample to lens. To calculate the solid angle ratio, we considered that the sample is in the origin of a sphere and the area ratio can be written as:

$$\beta = \frac{4\pi d^2}{\pi (r)^2} \tag{5.11}$$

In this equation, d is the distance between the sample and the lens, and r is the radius of the CaF_2 lens. We found β as 163.84 for our system. Afterwards, R, spectral area ratio is the ratio of the areas under the fluorescence and transmitted spectra.

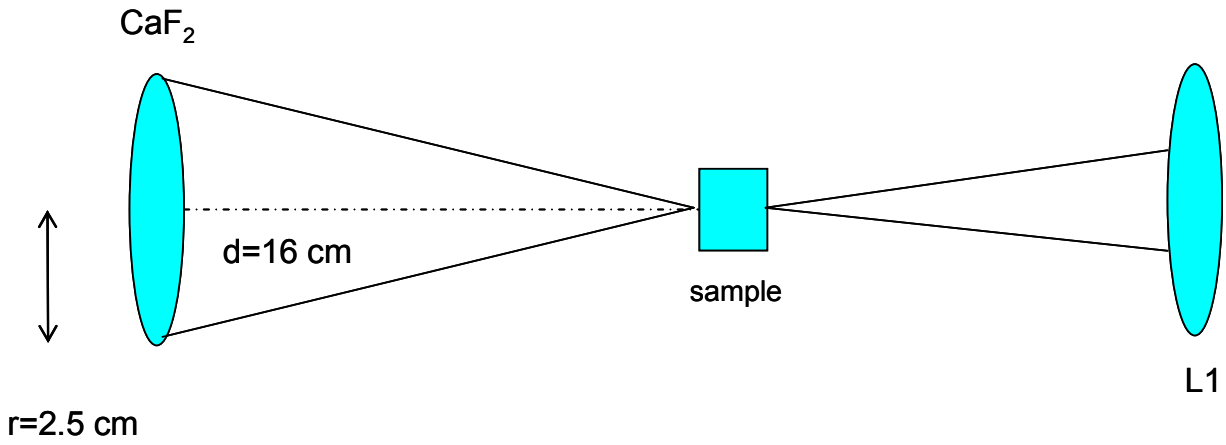

Figure 5.2: The used partition of the setup in order to find the solid angle ratio.

The transmitted spectrum was found after the two filters, Filter-77, and Filter-66. The values of R are changing for each sample and these are tabulated in Table 5.1. In order to find the resulting efficiency formula, P_{in} is written as:

$$P_{in} = P_{input} \times (1 - L_F) \times (1 - L_S) \tag{5.12}$$

P_{input} is the power of the incoming light through the sample. L_S is the scattered loss and L_F is the Fresnel reflection loss. We write the effect of the Fresnel loss only one time, because we investigate the power inside the sample and Fresnel loss can affect only one time. The resulting conversion efficiency measurements and other parameters are indicated in Table 5.1:

Sample Code	**Er^{3+}** (Weight %)	**L_S** (Scattering Loss)	I_i / I_T (Spectral Area Ratio)	**Average η_{eff}**
S1	0	0.85	4.75	0.012
S2	2.19	0.98	6.27	0.106
S3	4.22	0.99	6.14	0.192
S4	6.49	0.92	6.36	0.027
S5	10.86	0.92	5.99	0.016

Table 5.1: Average η_{eff} values including the values of R (spectral area ratios) and scattering losses.

In these calculations, we found the resulting η_{eff} values. In general, the transmitted intensity contains both of the effects of Fresnel loss and scattering loss. The maximal value of the

efficiency is 19 % approximately which is for S3 one. That S3 sample contains 4.22 weight % doping amount of erbium ions. Average scattering loss is 0.95 for erbium-doped samples. The loss value of the undoped sample is 0.85 which is small comparing doped ones.

In the next section, we will overview and evaluate the results of the colorimetric and fluorescence analysis.

Chapter 6

CONCLUSIONS

In this work, Er^{3+} doped elastomeric poly (ether-urethaneurea) copolymers (PUU) were prepared as UV-to-VIS converters. The samples were excited with ultraviolet light at 355 nm to investigate the spectroscopic qualities of polymer samples consisting of trivalent erbium ions with concentrations in the range 2.19% to 10.86% by weight. The broadband photoluminescence spectrum is obtained for erbium-doped samples. That is, for undoped one the emission spectrum is in the blue-green portion of the electromagnetic spectrum, however, for the trivalent erbium-doped one, the spectrum shifts to the red region which provides the extension of the spectrum from 400 to 750 nm and covers the entire spectrum. In the second part of the thesis, theory of color analysis is examined regarding the elements of visual system and their contributions to color perception. Then, various colorimetric measurement methods are defined, in order to comprehend the white light emission quality of our erbium-doped polymer samples. These include the determination of the (x, y) color coordinates, eye overlap index, color temperature, and color rendering index (CRI). The closest (x, y) color coordinate to the white region is (0.38, 0.43) which is for S2, 2.19 % by weight sample. Resulting CRI values are in the range of 57-70. These values are also close to the desired range of CRI values. Furthermore, sample S2 has the highest CRI value which is 70. These results indicate that the optimum weight percentage of trivalent erbium is around 2.2 weight % for the samples investigated in our research. Also, further increase in the erbium concentration increases the amount of self absorption and causes the departure of the color coordinates from the white region of the color chart. Additionally, the color temperatures of the polymer samples were in the range of 5093-5540 K. The value of η increases from 85% to 95% as the concentration of erbium is increased from 0 to 10.86% by weight. The change in η is caused by the self absorption bands of erbium around 430, 490, 523, and 660 nm. As a result, the emission band becomes narrower and the overlap becomes better in comparison with samples containing lower levels of erbium. We found the UV-to-VIS conversion efficiency which gives the ratio of incident power that is converted to visible fluorescence power. To find the

fluorescent power, we assumed that the polymer sample was a point radiating source. Both Fresnel losses and scattering losses were taken into account to estimate the conversion efficiency. The maximum determined conversion efficiency is 19 % for sample S3 containing 4.22 % by weight Er^{3+}.

These studies show that erbium-doped elastomeric poly (ether-urethaneurea) copolymers are potentially important new candidates for UV-VIS conversion applications and solid-state lighting.

BIBLIOGRAPHY

[1] P. E. Burrows, G. Gu, V. Bulovic, Z. Shen, S. R. Forrest, and M. E. Thompson, "Achieving full-color organic light-emitting devices for lightweight, flat-panel displays," *Ieee Transactions on Electron Devices*, vol. 44, pp. 1188-1203, 1997.

[2] B. V. Desphande R.S, Forrest S.R, "White-light-emitting organic electroluminescent devices based on interlayer sequential energy transfer," *Appl. Phys. Lett*, vol. 75, pp. 888-890, 1999.

[3] Z. Y. Xie, J. S. Huang, C. N. Li, S. Y. Liu, Y. Wang, Y. Q. Li, and J. C. Shen, "White light emission induced by confinement in organic multiheterostructures," *Applied Physics Letters*, vol. 74, pp. 641-643, 1999.

[4] S. Nizamoglu, T. Ozel, E. Sari, and H. V. Demir, "White light generation using CdSe/ZnS core-shell nanocrystals hybridized with InGaN/GaN light emitting diodes," *Nanotechnology*, vol. 18, pp. -, 2007.

[5] Y. Hamada, T. Sang, H. Fujii, Y. Nishio, H. Takanashi, and K. Shibata, "White-light-emitting material for organic electroluminescent devices," *Japanese Journal of Applied Physics Part 2-Letters*, vol. 35, pp. L1339-L1341, 1996.

[6] G. Heliotis, E. Gu, C. Griffin, C. W. Jeon, P. N. Stavrinou, M. D Dawson, and D. D. C. Bradley, "Wavelength-tunable and white-light emission from polymer-converted micropixellated InGaN ultraviolet light-emitting diodes," *Journal of Optics a-Pure and Applied Optics*, vol. 8, pp. S445-S449, 2006.

[7] J. Kido, K. Hongawa, K. Okuyama, and K. Nagai, "White Light-Emitting Organic Electroluminescent Devices Using the Poly(N-Vinylcarbazole) Emitter Layer Doped with Three Fluorescent Dyes," *Applied Physics Letters*, vol. 64, pp. 815-817, 1994.

[8] M. Suzuki, S. Tokito, M. Kamachi, K. Shirane, and F. Sato, "White light emission from polymer light-emitting devices based on blue and red phosphorescent polymers," *Journal of Photopolymer Science and Technology*, vol. 16, pp. 309-314, 2003.

[9] N. R. Mameno K., Suzuki K., Matsumoto S., Yamaguchi T.,Yoneda K., Hamada Y.,Kanno H., Nishino Y., Matsuoka H., Saito Y., Oima S., Mori N., Rajeswaran G., Mizukoshi S.,Hatwar T.K.,, *Proc. of Asia Display/IDW'02*, pp. 235, 2002.

[10] A. Misra, P. Kumar, M. N. Kamalasanan, and S. Chandra, "White organic LEDs and their recent advancements," *Semiconductor Science and Technology*, vol. 21, pp. R35-R47, 2006.

[11] R. H. Friend, R. W. Gymer, A. B. Holmes, J. H. Burroughes, R. N. Marks, C. Taliani, D. D. C. Bradley, D. A. Dos Santos, J. L. Bredas, M. Logdlund, and W. R. Salaneck, "Electroluminescence in conjugated polymers," *Nature*, vol. 397, pp. 121-128, 1999.

[12] C. W. Ko and Y.T.Tao, "Bright white organic light-emitting diode," *Applied Physics Letters*, vol. 79, 2001.

[13] K. O. Cheon and J. Shinar, "Bright white small molecular organic light-emitting devices based on a red-emitting guest-host layer and blue-emitting 4,4' - bis (2,2' - diphenylvinyl)-1,1' -biphenyl," *Applied Physics Letters*, vol. 81, 2002.

[14] E. M. Hosokawa C., Matsuura M., Fukuoka K., Nakamura H., Kusumoto T., "Organic multi-color electroluminescence display with fine pixels," *Synthetic Metals*, vol. 91, pp. 3-7, 1997.

[15] B. W. D'Andrade, M. A. Baldo, C. Adachi, J. Brooks, M. E. Thompson, and S. R. Forrest, "High-efficiency yellow double-doped organic light-emitting devices based

on phosphor-sensitized fluorescence," *Applied Physics Letters*, vol. 79, pp. 1045-1047, 2001.

[16] X. Gong, W. L. Ma, J. C. Ostrowski, G. C. Bazan, D. Moses, and A. J. Heeger, "White electrophosphorescence from semiconducting polymer blends," *Advanced Materials*, vol. 16, pp. 615-+, 2004.

[17] M. Godlewski, M. Skrobot, E. Guziewicz, and M. R. Phillips, "Color tuning of white light emission from thin films of ZnSe," *Journal of Luminescence*, vol. 125, pp. 85-91, 2007.

[18] M. Godlewski, E. Guziewicz, K. Kopalko, E. Lusakowska, E. Dynowska, M. M. Godlewski, E. M. Goldys, and M. R. Phillips, "Origin of white color light emission in ALE-grown ZnSe," *Journal of Luminescence*, vol. 102, pp. 455-459, 2003.

[19] M. Yamada, Y. Narukawa, H. Tamaki, Y. Murazaki, and T. Mukai, "A methodological study of the best solution for generating white light using nitride-based light-emitting diodes," *Ieice Transactions on Electronics*, vol. E88C, pp. 1860-1871, 2005.

[20] H. S. Chen, D. M. Yeh, C. F. Lu, C. F. Huang, W. Y. Shiao, J. J. Huang, C. C. Yang, I. S. Liu, and W. F. Su, "White light generation with CdSe-ZnS nanocrystals coated on an InGaN-GaN quantum-well blue/green two-wavelength light-emitting diode," *Ieee Photonics Technology Letters*, vol. 18, pp. 1430-1432, 2006.

[21] H. S. Chen, C. K. Hsu, and H. Y. Hong, "InGaN-CdSe-ZnSe quantum dots white LEDs," *Ieee Photonics Technology Letters*, vol. 18, pp. 193-195, 2006.

[22] D. Matsuura, "Red, green, and blue upconversion luminescence of trivalent-rare-earth ion-doped Y2O3 nanocrystals," *Applied Physics Letters*, vol. 81, pp. 4526-4528, 2002.

[23] L. D. Carlos, Y. Messaddeq, H. F. Brito, R. A. S. Ferreira, V. D. Bermudez, and S. J. L. Ribeiro, "Full-color phosphors from europium(III)-based organosilicates," *Advanced Materials*, vol. 12, pp. 594-598, 2000.

[24] B. Damilano, N. Grandjean, F. Semond, J. Massies, and M. Leroux, "From visible to white light emission by GaN quantum dots on Si(111) substrate," *Applied Physics Letters*, vol. 75, pp. 962-964, 1999.

[25] J. Liu, Y. J. Shi, and Y. Yang, "Improving the performance of polymer light-emitting diodes using polymer solid solutions," *Applied Physics Letters*, vol. 79, pp. 578-580, 2001.

[26] D. A. Steigerwald, J. C. Bhat, D. Collins, R. M. Fletcher, M. O. Holcomb, M. J. Ludowise, P. S. Martin, and S. L. Rudaz, "Illumination with solid state lighting technology," *Ieee Journal of Selected Topics in Quantum Electronics*, vol. 8, pp. 310-320, 2002.

[27] J. Lee, V. C. Sundar, J. R. Heine, M. G. Bawendi, and K. F. Jensen, "Full color emission from II-VI semiconductor quantum dot-polymer composites," *Advanced Materials*, vol. 12, pp. 1102-+, 2000.

[28] U. Demirbas, A. Kurt, A. Sennaroglu, E. Yilgor, and I. Yilgor, "Luminescent Nd^{3+} doped silicone-urea copolymers," *Polymer*, vol. 47, pp. 982-990, 2006.

[29] L. S. P. Frank L. Pedrotti, *Introduction to Optics*, Second Edition ed. New Jersey: Prentice Hall, 1993.

[30] S. Y. Koeppen C. , G. Jiang, A.F. Garito, Larry R. Dalton, *J.Opt. Soc. Am. B.*, vol. 14, 1997.

[31] M. J. A. d. D. Slooff L.H. , A. van Blaaderen, A. Polman, *Appl. Phys. Lett.*, vol. 76, 2000.

[32] K. Kuriki, Y. Koike, and Y. Okamoto, "Plastic optical fiber lasers and amplifiers containing lanthanide complexes," *Chemical Reviews*, vol. 102, pp. 2347-2356, 2002.

[33] T. Danger, J. Koetke, R. Brede, E. Heumann, G. Huber, and B. H. T. Chai, "Spectroscopy and Green up-Conversion Laser-Emission of Er(3+)-Doped Crystals at Room-Temperature," *Journal of Applied Physics*, vol. 76, pp. 1413-1422, 1994.
[34] J. A. Gonzalez-Ortega, E. M. Tejeda, N. Perea, G. A. Hirata, E. J. Bosze, and J. McKittrick, "White light emission from rare earth activated yttrium silicate nanocrystalline powders and thin films," *Optical Materials*, vol. 27, pp. 1221-1227, 2005.
[35] S. J. Sangwine and R. E. N. H. , *The color image processing handbook*: Springer, 1998.
[36] S. W. S. Wyszecki G., *Color Science, 'Concepts and Methods, quantitative data and formulae*. New York: John Wiley& Sons, 2000.
[37] S. K. Shevell, *The Science of Color*: Elsevier, 2003.
[38] K.-N. Liou, *An Introduction to Atmospheric Radiation*, vol. 84, 2nd edition ed, 2002.
[39] W. Kemp, *Organic Spectroscopy*. New York: W.H.Freeman, 1991.
[40] D. S. Davis A. , *Weathering of Polymers*: Springer, 1983.
[41] A. L. Andrady, *Plastics and the Environment*: Wiley-IEEE, 2003.
[42] B. G. Lipták, *Instrument Engineers' Handbook*: CRC Press.
[43] R. Macomber, *Organic Chemistry*, 1996.
[44] E. Desurvire, *Erbium-Doped Fiber Amplifiers, Principles and Applications*. Toronto: John Wiley&Sons, 1994.
[45] K. Pátek, *Glass Lasers*. London: CRC Press, 1970.
[46] R. Reisfeld, *Radiative and non-radiative transitions of rare-earth ions in glass*, vol. 22. New York: Springer-Verlag.
[47] W. M. J. Riseberg L.A., *Relaxation phenomena in rare earth luminescence*, vol. 14. Amsterdam: North Holland Publishing Co., 1976.
[48] W. J. Miniscalco, "Erbium-Doped Glasses for Fiber Amplifiers at 1500-Nm," *Journal of Lightwave Technology*, vol. 9, pp. 234-250, 1991.
[49] E. F. Schubert, *Light emitting diodes*: Cambridge University press, 2003.
[50] G. Sharma, *Digital Color Imaging Handbook*: CRC Press, 2003.
[51] R. R. Robert Eisberg, *Quantum Physics of Atoms, Molecules, Solids, Nuclei and Particles*: John Wiley&Sons, 1985.
[52] G. Woods, *The ICI Polyurethanes Book*. New York: John Wiley, 1990.
[53] N. M. K. Lambla, K. A. Woodhouse, and S. L. Cooper, *Polyurethanes in Biomedical Applications*. Boca Raton, FL, USA: CRC Press, 1988.
[54] A. Yariv, *Optical Electronics in Modern Communications*, Fifth Edition ed. New York: Oxford University Press, 1997.
[55] E. Hecht, *Optics*, 2nd edition ed. Canada: Addison Wesley, 1988.
[56] J. S. Götz Hoeppe, *Why the sky is blue: Discovering the Color of Life*: Princeton University Press, 2007.
[57] http://www.newport.com/Optical-Radiation-Terminology-and-Units/381842/1033/catalog.aspx
[58] http://cvrl.ioo.ucl.ac.uk/database/data/cmfs/ciexyz64_1.txt